NASA TECHNICAL MEMORANDUM

NASA TM X-1910

NASA TM X-1910

FLIGHT TEST OF HIGH-DENSITY PHENOLIC-NYLON ON A SPACECRAFT LAUNCHED BY THE PACEMAKER VEHICLE SYSTEM

by William G. Witte

Langley Research Center
Langley Station, Hampton, Va.

NATIONAL AERONAUTICS AND SPACE ADMINISTRATION • WASHINGTON, D. C. • NOVEMBER 1969

DISCLAIMER NOTICE

THIS DOCUMENT IS BEST QUALITY AVAILABLE. THE COPY FURNISHED TO DTIC CONTAINED A SIGNIFICANT NUMBER OF PAGES WHICH DO NOT REPRODUCE LEGIBLY.

1. Report No. NASA TM X-1910	2. Government Accession No.	3. Recipient's Catalog No.
4. Title and Subtitle FLIGHT TEST OF HIGH-DENSITY PHENOLIC-NYLON ON A SPACECRAFT LAUNCHED BY THE PACEMAKER VEHICLE SYSTEM		5. Report Date November 1969 6. Performing Organization Code
7. Author(s) William G. Witte		8. Performing Organization Report No. L-6678 10. Work Unit No. 709-09-00-01-23
9. Performing Organization Name and Address NASA Langley Research Center Hampton, Va. 23365		11. Contract or Grant No. 13. Type of Report and Period Covered Technical Memorandum
12. Sponsoring Agency Name and Address National Aeronautics and Space Administration Washington, D.C. 20546		14. Sponsoring Agency Code

15. Supplementary Notes

16. Abstract

High-density phenolic-nylon material was flight tested on a recoverable spacecraft launched by the Pacemaker vehicle system. The spacecraft was a hemispherically blunted cone with a cylindrical afterbody. The overall dimensions were a length of 29.5 inches (74.9 cm) and a diameter of 10 inches (25.4 cm). Ablation performance data on the phenolic-nylon were obtained by the use of ablation sensors and thermocouples and by post-flight profile-change measurements. Profile-change measurements were also obtained for several panels of low-density materials attached to the spacecraft cylinder. A comparison of measured heating rates with computed turbulent and laminar heating rates indicated that the boundary layer underwent transition.

17. Key Words Suggested by Author(s) Ablation performance High-density phenolic-nylon	18. Distribution Statement Unclassified – Unlimited		
19. Security Classif. (of this report) Unclassified	20. Security Classif. (of this page) Unclassified	21. No. of Pages 53	22. Price* $3.00

*For sale by the Clearinghouse for Federal Scientific and Technical Information Springfield, Virginia 22151

FLIGHT TEST OF HIGH-DENSITY PHENOLIC-NYLON ON A SPACECRAFT LAUNCHED BY THE PACEMAKER VEHICLE SYSTEM

By William G. Witte
Langley Research Center

SUMMARY

High-density phenolic-nylon material was flight tested on a recoverable spacecraft launched by the Pacemaker vehicle system. The spacecraft was a hemispherically blunted cone with a cylindrical afterbody. The overall dimensions were a length of 29.5 inches (74.9 cm) and a diameter of 10 inches (25.4 cm). Ablation performance data on the phenolic-nylon were obtained by the use of ablation sensors and thermocouples and by post-flight profile-change measurements.

Profile-change measurements were also obtained for several panels of low-density materials attached to the spacecraft cylinder.

A comparison of measured heating rates with computed turbulent and laminar heating rates indicated that the boundary layer underwent transition.

Flight data and computed test conditions are presented.

INTRODUCTION

High-density phenolic-nylon was the standard high-density charring ablator used in correlating the plasma-arc-heater facilities in the round-robin study monitored by Stanford Research Institute (see ref. 1). As a result of the considerable interest in obtaining flight data on this material, the present flight test (one in a series of Materials Technology Experiments) was conducted. As in previous tests, the spacecraft containing the experiments was launched by a Pacemaker vehicle from NASA Wallops Station. At the end of the flight the spacecraft was recovered from the ocean.

The primary purpose of the test was to obtain ablation performance data on the high-density phenolic-nylon material. The data were obtained by the use of ablation sensors and thermocouples and by post-flight measurements of surface recession. In addition to the primary ablation experiment, secondary experiments consisted of the post-flight measurement of surface recession on several panels of low-density materials attached to the spacecraft cylinder and the detection of boundary-layer transition with the use of calorimeters.

The data obtained from these experiments are presented in this paper.

SYMBOLS

M_∞	free-stream Mach number
p_e	local surface pressure
p_{SL}	standard pressure at sea level
$p_{t,2}$	total pressure behind a normal shock
p_∞	free-stream pressure
r_n	nose radius
s	distance along surface measured from stagnation point
T_∞	free-stream temperature
ρ_{SL}	standard density at sea level
ρ_∞	free-stream density
ϕ	circumferential location

SPACECRAFT

The spacecraft (see fig. 1) was a hemispherically blunted cone with a cylindrical afterbody. The overall dimensions were a length of 29.5 inches (74.9 cm) and a diameter of 10 inches (25.4 cm). The effective nose radius was 3.83 inches (9.73 cm) and the half-angle of the cone was 6.25°. The primary structure was 0.062-inch (0.1575-cm) inconel in the hemisphere-cone region and 0.075-inch (0.1905-cm) 7075 aluminum alloy in the cylinder region.

Cylindrical sections aft of the spacecraft housed a recovery parachute and the spacecraft telemetry. Figures 2(a) and 2(b) are photographs of the spacecraft and these cylindrical sections, assembled and disassembled.

The thermal protection material on the hemisphere, cone, and forward portion of the cylinder was high-density phenolic-nylon. The hemisphere-cone section was molded

in one piece. The cone-cylinder shoulder section and the cylindrical section were machined from molded billets of the material. The size of the molded billets required these sections to be machined in two pieces rather than in one piece.

The hemisphere-cone is detachable from the cylinder at the separation plane in the cone (see fig. 1). This arrangement facilitated the assembly of the instrumentation. In order to avoid flow and erosion problems at the separation plane, the outer cone of phenolic-nylon was extended onto the cylindrical section. Thus the separation plane was located 2.25 inches (5.72 cm) forward of the cone-cylinder shoulder.

The density of the phenolic-nylon on this spacecraft was 75.0 lb/ft^3 (1201 kg/m^3). The composition of the material was 50 percent by weight phenolic and 50 percent by weight finely ground nylon. The same standardized procedures used for making models for the Stanford Research Institute (SRI) correlation in reference 1 were followed to ensure that the spacecraft material was identical to the phenolic-nylon used in the SRI tests. These procedures entailed careful measuring and mixing of the material constituents as well as accurate timing and temperature and pressure control during the various steps of the molding process. After molding, final checks of the material were made by taking X-rays to examine for voids and by measuring the density.

The aft portion of the cylinder was covered with six longitudinal panels of low-density add-on materials (see fig. 2(a)). There were two panels, mounted 180^o apart, of each of these three materials: teflon foam, filled silicone elastomer, and foamed quartz. The panels were backed up by a 0.25-inch (0.635-cm) layer of cork, which would have provided sufficient thermal protection to the primary structure in case of failure of any of the panels. Three antenna windows, roughly 2 by 3 inches (5.08 by 7.62 cm) in size, and a teflon patch, roughly 2 by 1.5 inches (5.08 by 3.81 cm) in size, were installed in cutouts in the add-on panels. Table I presents the locations of these panels and inserts. The densities of these materials are as follows:

Material (manufacturer)	Density	
	lb/ft^3	kg/m^3
Teflon foam (Avco Corp.)	32	513
Filled silicone elastomer, Mod 5 (Avco Corp.)	42	673
Foamed quartz, LI-15 (Lockheed Aircraft Corp.)	15	240
Antenna windows, Avcoat II (Avco Corp.)	62	993
Teflon	130	2082

The phenolic-nylon was bonded to the primary structure with an elastomeric silicone rubber adhesive to permit differential expansion and contraction to occur between the phenolic-nylon and the structure without cracking the phenolic-nylon. The same

adhesive was used to bond the add-on panels to the cork and to bond the joints between the panels, sections, and inserts. These elastomeric seams were approximately 0.030 to 0.060 inch (0.0762 to 0.15240 cm) wide. The separation plane was not bonded.

INSTRUMENTATION

The instrumentation located in the phenolic-nylon portion of the spacecraft consisted of the following: six 4-element dual ablation rate sensors, six 4-element spring-wire ablation rate sensors, four 3-element thermocouple plugs, and three calorimeters.

Table I presents the exact locations of this instrumentation.

Both the spring-wire ablation rate sensors (ref. 2) and the dual ablation rate sensors measure surface recession events. A dual sensor is essentially a spring-wire ablation rate sensor used in conjunction with a platinum ground wire, with the spring-wire tube and the platinum ground wire forming the elements of a make-wire sensor (ref. 2). Table II presents the sensing depths of the elements in all the sensors. The spring-wire tubes in the nose cap were type 304 stainless steel. The spring-wire tubes in the cylinder were 7075 aluminum. Both the spring-wire sensors and the make-wire sensors have been used successfully in previous Pacemaker tests.

The four thermocouple plugs were used to obtain surface and in-depth temperatures. Figure 3 is a sketch of a typical thermocouple plug showing a surface thermocouple and an in-depth thermocouple. The sensing tip is formed of thermocouple wires flattened to ribbons 0.002 inch (0.051 mm) thick and 0.060 inch (1.52 mm) wide. The ribbons are then insulated from each other and from the tapered pin sections by mica sheets of 0.0002-inch (0.005-mm) thickness. This assembly of ribbons, mica, and split-pin sections is pressed into a matched tapered hole. These plugs are installed in the spacecraft with the planes of the ribbons normal to the expected stream flow. Initially, the thermal junctions are formed by grinding and polishing across the sensing tip. This action flows metal across the compressed mica insulation. During ablation, aerodynamic shear bends the upstream ribbon over to form the junction with the downstream ribbon. These thermocouples provide instantaneous and continuous reading data. In this test, however, the data were commutated. Table III presents the initial sensing depths of the three elements in each plug. The ribbons of the thermocouples at the 45° station and cone station 1 were tungsten and tungsten with 26 percent rhenium. The thermocouples at cone station 2 and cylinder station 1 had chromel and alumel ribbons.

The calorimeters were located on the spacecraft cylinder. Calorimeter C-1, at cylinder station 1, was placed with its sensing area flush with the ablator surface. Calorimeters C-2 and C-3, at cylinder station 2, were placed with their sensing areas recessed 0.010 inch (0.0254 cm) below the ablator surface in the event that greater

ablation occurred than was predicted. In such a case, hot gases would have impinged upon the side of the flush calorimeter and caused inaccuracies in its output. The calorimeters were of the thin-foil type (ref. 3). The thermal sensing area was a 0.011-inch-thick (0.28-mm), 0.132-inch-diameter (3.35-mm) circular plate of constantan foil over a dead airspace. The plate had a high-emissivity graphitic coating. The edge of the plate was in contact with a copper heat sink located under the heat shield. This heat sink maintained the edge at a constant and low temperature. The juncture of the edge with the heat sink formed the cold junction of a copper-constantan differential thermocouple. A copper wire attached to the center of the constantan plate formed the hot junction of the thermocouple. This copper wire and a lead from the heat sink were attached to a device for measuring electromotive force (emf). During heating, when a temperature differential exists between the edge and the center of the constantan foil, an emf is generated. The incident heat flux on the foil is derived from the emf. This heating rate is essentially a cold-wall heating rate.

In addition to the instrumentation in the phenolic-nylon, five structural thermocouples were spot welded to the inside of the hemisphere-cone primary structure. These thermocouples monitored the internal temperature of the spacecraft during the test. They were located at the stagnation point, at the 22.5°, 45°, and 67.5° stations, and at a point near the separation plane.

A standard Inter-Range Instrumentation Group (IRIG) FM/FM telemetry system was housed in the cylindrical section aft of the parachute section. It consisted of seven IRIG proportional subcarrier channels – four channels for vehicle performance obtained from four accelerometers located in this cylindrical section and three channels for experimental data. The telemeter monitored 32 of the 48 spring-wire sensor events. The remaining 16 sensor events, plus 28 others, were recorded on an event recorder (see ref. 4) located in the spacecraft cylinder. This event recorder was recovered with the spacecraft.

LAUNCH VEHICLE AND OPERATIONS

The Pacemaker launch vehicle and spacecraft in launch position are shown in figure 4. The vehicle was launched June 27, 1968, from the NASA Wallops Station launch facility. It was launched at an elevation angle of 73.3° on an azimuth of 147°.

The propulsion system of the Pacemaker launch vehicle consisted of four stages of solid-propellant rocket motors: Honest John, Nike, TX-77, and Recruit. All stages were ignited during vehicle ascent. The first stage was ground fired. After burnout it was drag separated. The second stage was ignited by an on-board programer with a dual ignition system. It was blast separated upon ignition of the third stage. An on-ground computer was used to command fire the third stage. A pressure switch operated by the

chamber-pressure decay of the third stage fired the fourth stage. The third stage was blast separated upon ignition of the fourth stage.

After fourth-stage burnout the spacecraft decelerated to subsonic speeds. At an altitude of roughly 10 000 feet (3048 meters), a barometric switch actuated two pyrotechnic delay squibs to ignite a separation motor that accelerated the spacecraft away from the fourth stage and, 0.25 second later, to ignite tumble motors mounted in the fourth stage normal to the flight axis and thereby cause the fourth stage to cartwheel. The increased drag of the fourth stage then caused it to take a different trajectory than the one being taken by the spacecraft. At roughly 8500 feet (2590 meters) a radar reflective parachute was deployed from the spacecraft to lower it to the surface of the water where it was recovered. Figure 5 is a photograph of the recovered spacecraft.

A plot of the trajectory and the sequence of events are shown in figure 6. The variations of flight velocity and altitude during the data period determined from radar tracking data are shown in figure 7. A C-band tracking radar transponder in the spacecraft facilitated tracking. Telemetered normal and transverse accelerometer data showed no apparent body motions during the data period. The total angle of attack during the data period was less than 3°. The roll rate at third-stage burnout, obtained from a gyro, was 25°/sec.

TEST ENVIRONMENT

A rawinsonde that was launched prior to flight measured ambient pressure and temperature. These values and the computed ambient density are shown in figure 8.

Computed pressure distributions over the initial spacecraft configuration are shown in figure 9 for several free-stream Mach numbers. The distributions for the hemisphere and cone were obtained from reference 5, and the distribution for the cylinder was obtained by the method of characteristics.

Computed time histories of cold-wall heating rates, local Mach numbers, stagnation enthalpy, local Reynolds numbers, local pressures, and local turbulent shear are presented in figures 10 to 15. These computations were made for the actual flight trajectory by the methods described in reference 6. The wiggles in the initial portions of the local Mach number histories (fig. 11) are due to the rapidly changing conditions during third-stage thrusting as free-stream Mach numbers increase from subsonic to hypersonic values.

Calorimeter heating rates and indications of transition are discussed subsequently in the section "Calorimeter Results."

RESULTS AND DISCUSSION

Spacecraft Appearance

The phenolic-nylon ablated almost symmetrically about the spacecraft center line, with slightly greater recession at the 45° station than at the stagnation point. After the test, on the hemisphere, the ablation wires and tubes protruded up to 0.27 inch (0.7 cm) above the surface. Figure 16 is a closeup photograph of the hemisphere showing some of the protruding tubes and wires.

There were large cracks in the phenolic-nylon material, especially on the cone and cylinder. In several areas the heat shield had pulled away from and lifted off the primary structure (see fig. 17). It is assumed that the cracks started to form when the material cooled during the parachute descent. In some unreported ground facility tests of phenolic-nylon, cracking occurred during cooling of the material to room temperature after testing. Often the cracks enlarged for several hours after the material reached room temperature, apparently relieving the internal stresses that developed in the material during cooling. On this recovered spacecraft, however, a delayed enlarging of the cracks was not noted.

At the separation plane no unusual or excessive ablation occurred, although that joint was not bonded.

Surface Recession Results

The recession data measured during the flight are presented in figure 18 and table II. These data represent the successful operation of 15 of the 16 make-wire elements in the dual sensors and 29 of the 32 spring-wire sensors located in the phenolic-nylon material in the hemispherical region of the spacecraft. None of the sensors located in the phenolic-nylon material in the cylindrical portion of the spacecraft were triggered. The average total recession (ATR) indicated in figure 18 was determined from post-flight measurement of the spacecraft using the dial-gage apparatus described in reference 7. The average total recession was 0.34 inch (0.864 cm) at the stagnation point and 0.42 inch (1.067 cm) at the 45° station on the hemispherical nose cap. With the dial-gage apparatus, distances from the fixture to the spacecraft surface were measured at selected locations before and after testing. The fixture enables the measurements to be repeated at the same locations. The difference between the before and after measurements is the profile change. Results are shown in figure 19 for several longitudinal locations (spacecraft stations and surface distances) at 12 circumferential locations. For a given location on the cone or cylinder, the profile change may be either positive or negative depending on whether surface recession or expansion has occurred. Under certain conditions surface expansion due to either

swelling of the heat shield or condensation of pyrolysis products on the heat-shield surface can occur. Although recession of the ablation surface is expected in the present test, apparent surface expansion due to lifting of the heat shield from the primary structure occurred. Those portions of the cone and cylinder where the separation was obvious are indicated by ×'s in figures 19(b), 19(c), and 19(d). A section cut from the spacecraft shows separation in the cone and cylinder, but indicates that the bond between hemisphere and primary structure was intact. (See fig. 17.)

An indication of the final char thickness was obtained from the section of phenolic-nylon cut from the recovered spacecraft. (See fig. 17.) Char thicknesses measured with a scale are noted in this figure.

In addition to the longitudinal measurements, measurements were made around the 30°, 40°, 50°, 60°, and 70° stations on the hemisphere. These results are shown in figure 20. Some of the ridges and depressions extend longitudinally from the 30° to 70° stations. They are most noticeable at the 40°, 50°, and 60° stations. The arithmetic means of the surface recession and the standard deviations from the means are as follows:

Station	Surface recession, in. (mm)	
	Arithmetic mean	Standard deviation
30°	0.365 (9.27)	0.016 (0.41)
40°	.416 (10.57)	.020 (0.51)
50°	.447 (11.35)	.031 (0.79)
60°	.406 (10.31)	.015 (0.38)
70°	.290 (7.37)	.010 (0.25)

Of the three add-on materials (see fig. 19), the filled silicone elastomer and foamed quartz showed a minimal amount of recession or shrinkage. Each of the teflon foam panels showed a maximum recession of 0.030 to 0.040 inch (0.0762 to 0.1016 cm). Sections cut from the recovered spacecraft showed no separation of the bond on the add-on panels.

Temperature Results

The thermocouple plug at the 45° station ablated more than the surrounding material. The resulting indentation was about 0.25 inch (0.635 cm) deep. The thermocouple ribbons protruded above the surface at this location. The tips of the ribbons were partly melted. Downstream effects on ablation due to the indentation were minor. The temperature histories obtained for the 45° station are not presented in their entirety because they do not represent actual temperatures at the desired locations. Figure 21 presents the initial portion of the surface temperature history. Beyond 72.2 seconds the data were not reliable. The thermocouple plugs in the cone and cylinder ablated smoothly with the

surrounding surfaces. Temperature-time histories obtained from the cone and cylinder thermocouples are shown in figure 22. The surface temperatures shown here should be interpreted carefully. They do not rise and fall with the heating rates, as might be expected. Rather, they rise sharply with the heating rate to some value and then level off for the duration of the heating period.

The five structural thermocouples inside the hemisphere-cone showed no temperature rise during the flight test.

Calorimeter Results

The time history of heating rate obtained from calorimeter C-1 at cylinder station 1 is shown in figure 23. The computed laminar and turbulent heating rates have been superimposed on the calorimeter heating rate in order to obtain the time of boundary-layer transition. Up to 69 seconds the calorimeter heating rate is of the order of magnitude of the computed laminar heating rate, at 70 seconds the heating rate is in transition, and by 71 seconds the calorimeter heating rate starts to exceed the laminar and approaches the turbulent heating rate. The heating rate is approximately two-thirds the computed turbulent rate from peak heating until roughly 85 seconds. At this time the calorimeter heating rate approaches the computed laminar heating rate. The local Reynolds number has been decreasing and at 85 seconds has dropped below 3.5×10^5.

Additional evidence to support the time of transition from laminar to turbulent heating can be seen in figure 21. This surface temperature-time history at the 45° station shows every data point between 69.2 and 72.2 seconds. The sharp rise in temperature starting at 71.3 seconds indicates this is the time of transition at the 45° station.

The data from calorimeters C-2 and C-3 were lost in transmission because of faulty amplifiers.

CONCLUDING REMARKS

High-density phenolic-nylon material was flight tested on a recoverable spacecraft launched by the Pacemaker vehicle system. Ablation performance data on the phenolic-nylon were obtained by the use of ablation sensors and thermocouples and by profile-change measurements. The average total recession was 0.34 inch (0.864 cm) at the stagnation point and 0.42 inch (1.067 cm) at the 45° station on the hemispherical nose cap.

Profile-change measurements were also obtained for several panels of low-density materials attached to the spacecraft cylinder. Foamed quartz and filled silicone elastomer showed a minimal amount of recession or shrinkage. The teflon foam panels showed a maximum recession of 0.030 to 0.040 inch (0.0762 to 0.1016 cm).

A comparison of measured heating rates with computed turbulent and laminar heating rates indicated that the boundary layer underwent transition.

Langley Research Center,
National Aeronautics and Space Administration,
Langley Station, Hampton, Va., August 29, 1969.

REFERENCES

1. Hiester, Nevin K.; and Clark, Carroll F.: Comparative Evaluation of Ablating Materials in Arc Plasma Jets. NASA CR-1207, 1968.

2. LeBel, Peter J.; and Russell, James M., III: Development of Sensors to Obtain In-Flight Ablation Measurements of Thermal-Protection Materials. NASA TN D-3683, 1966.

3. Malone, Erle W.: Design and Calibration of Thin Foil Heat Flux Sensors. Preprint No. P6-2-PHYMMID-67, Instrum. Soc. Amer., 1967.

4. Russell, James M., III: An Event Recorder for Obtaining Missile Heat-Shield Ablation Data. Preprint No. P8-1-PHYMMID-67, Instrum. Soc. Amer., 1967.

5. Arnold, John W.; Simmons, Harmon L.; and Miller, William T.: An Investigation of the Aerodynamic Characteristics of a 25° Sphere-Cone Including a Pressure Distribution Analysis at Angles of Attack, and a Trajectory Analysis During a Typical Reentry Trajectory. Rep. No. NASA CR-66037, LTV Aerospace Corp., [1966].

6. Graves, Randolph A., Jr.; and Witte, William G.: Flight-Test Analysis of Apollo Heat-Shield Material Using the Pacemaker Vehicle System. NASA TN D-4713, 1968.

7. Walton, Thomas E., Jr.; Witte, William G.; and O'Hare, Brian J.: Flight Investigation of the Effects of Apollo Heat-Shield Singularities on Ablator Performance. NASA TN D-4791, 1968.

TABLE I.- LOCATION OF INSTRUMENTATION AND ADD-ON MATERIALS

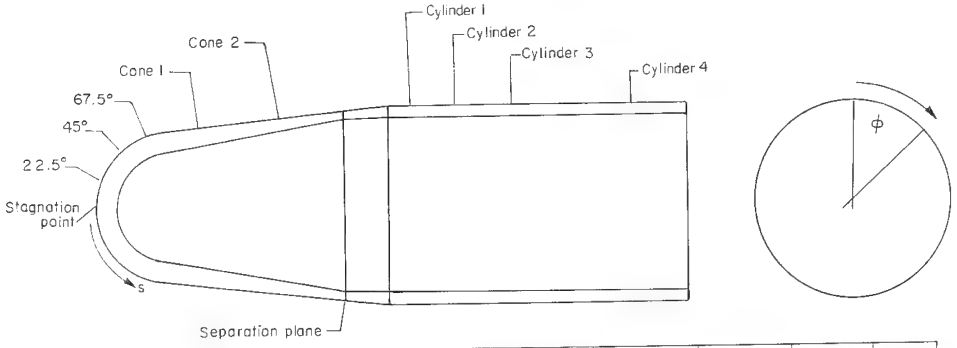

Circumferential location, ϕ (a)	Spacecraft station	Surface distance, s, in. (cm)	Dual ablation sensor	Spring-wire sensor	3-element thermocouple plugs	Calorimeter	Add-on ablator	C-band antenna window
0°	Stagnation point	0	Yes					
	22.5°	1.5 (3.81)		Yes				
	45°	3.0 (7.62)			Yes			
	67.5°	4.5 (11.43)	Yes					
0° to 60°		21.03 to 32.03 (53.4 to 81.4)					Filled silicone elastomer	
6°		0 to 30.0 (0 to 76.2)						
23°		0 to 30.0 (0 to 76.2)						
40° to 80°		28.78 to 30.78 (73.1 to 78.1)						Yes
60°	67.5°	4.5 (11.43)		Yes				
60° to 120°		21.03 to 32.03 (53.4 to 81.4)					Foamed quartz	
66°		0 to 30.0 (0 to 76.2)						
70°	Cylinder 1	17.72 (45.0)	Yes					
83°		0 to 30.0 (0 to 76.2)						
110°	Cylinder 2	19.72 (50.1)				C-3		
120°	45°	3.0 (7.62)		Yes				
	67.5°	4.5 (11.43)		Yes				
120° to 140°		28.78 to 30.78 (73.1 to 78.1)					Teflon patch	
120° to 180°		21.03 to 32.03 (53.4 to 81.4)					Teflon foam	
126°		0 to 30.0 (0 to 76.2)						
143°		0 to 30.0 (0 to 76.2)						
160° to 200°		28.78 to 30.78 (73.1 to 78.1)						Yes
180°	22.5°	1.5 (3.81)	Yes					
	67.5°	4.5 (11.43)		Yes				
	Cone 1	7.18 (18.24)			Yes			
180° to 240°		21.03 to 32.03 (53.4 to 81.4)					Filled silicone elastomer	
186°		0 to 30.0 (0 to 76.2)						
203°		0 to 30.0 (0 to 76.2)						
210°	Cone 2	11.20 (28.43)			Yes			
240°	45°	3.0 (7.62)		Yes				
240° to 300°		21.03 to 32.03 (53.4 to 81.4)					Foamed quartz	
246°		0 to 30.0 (0 to 76.2)						
250°	Cylinder 2	19.72 (50.1)	Yes					
263°		0 to 30.0 (0 to 76.2)						
270°	Cylinder 1	17.72 (45.0)				C-1		
280° to 320°		28.78 to 30.78 (73.1 to 78.1)						Yes
290°	Cylinder 2	19.72 (50.1)				C-2		
300°	45°	3.0 (7.62)	Yes					
300° to 360°		21.03 to 32.03 (53.4 to 81.4)					Teflon foam	
306°		0 to 30.0 (0 to 76.2)						
315°	Cylinder 1	17.72 (45.0)			Yes			
323°		0 to 30.0 (0 to 76.2)						

[a]Circumferential locations are measured clockwise, looking at the spacecraft from the front.

TABLE II.- ABLATION DATA

(a) Make-wire ablation rate sensor data

Spacecraft station	Circumferential location, ϕ	Sensing depth, in. (cm)	Time triggered, sec (a)
Stag point	0^{o}	0.015 (0.038)	71.80
		.040 (.102)	73.41
		.140 (.356)	88.24
		.290 (.737)	136.45
22.5^{o}	180^{o}	0.005 (0.013)	71.75
		.110 (.279)	84.59
		.365 (.927)	N.T.
		.290 (.737)	132.87
45^{o}	300^{o}	0.010 (0.025)	72.09
		.036 (.091)	73.37
		.090 (.229)	76.37
		.270 (.686)	92.79
67.5^{o}	0^{o}	0.004 (0.010)	72.85
		.024 (.061)	75.52
		.240 (.610)	118.62
		.064 (.163)	81.33
Cylinder 1	70^{o}	0.000 (0.000)	N.T.
		.025 (.064)	N.T.
		.050 (.127)	N.T.
		.090 (.229)	N.T.
Cylinder 2	110^{o}	0.000 (0.000)	N.T.
		.025 (.064)	N.T.
		.050 (.127)	N.T.
		.090 (.229)	N.T.

[a]N.T. denotes that the make-wire sensor was unaffected by flight (i.e., not triggered).

TABLE II.- ABLATION DATA – Concluded

(b) Spring-wire ablation rate sensor data

Spacecraft station	Circumferential location, ϕ	Sensing depth, in. (cm) (a)	Time triggered, sec (b)		
			Event-recorder data		Telemetered data
			Earliest	Latest	
Stag point	0°	0.035 (0.089)	76.27	76.29	76.28
		.060 (.152)	82.97	82.98	83.06
		.160 (.406)	92.64	92.68	N.T.
		.310 (.787)	N.T.	N.T.	N.T.
22.5°	180°	0.025 (0.064) (thru)	74.01	74.02	74.00
		.130 (.330)	106.81	106.84	106.81
		.385 (.978)	N.T.	N.T.	N.T.
		.310 (.787)	N.T.	N.T.	N.T.
22.5°	0°	0.026 (0.066) (thru)	73.57	73.58	73.61
		.259 (.658)	N.T.	N.T.	N.T.
		.045 (.114)	76.94	77.03	Not TM
		.085 (.216)	84.04	84.07	84.17
45°	120°	0.046 (0.117)	74.63	74.64	Not TM
		.145 (.368)	82.82	82.83	Not TM
		.610 (1.549)	N.T.	N.T.	Not TM
		.760 (1.930)	N.T.	N.T.	N.T.
45°	240°	0.030 (0.076)	74.75	74.76	74.79
		.086 (.218)	76.09	76.11	76.15
		.185 (.470) (thru)	87.82	87.84	88.01
		.450 (1.143)	N.T.	N.T.	N.T.
45°	300°	0.035 (0.089) (thru)	73.37	73.43	73.89
		.056 (.142)	74.71	74.72	74.77
		.110 (.279)	79.40	79.45	79.49
		.290 (.737)	123.96	124.05	123.82
67.5°	0°	0.024 (0.061)	80.96	80.98	80.95
		.044 (.112)	81.42	81.45	81.54
		.260 (.660)	98.28	98.37	Not TM
		.084 (.213)	Not Rec	Not Rec	82.04
67.5°	120°	0.030 (0.076)	83.39	83.41	83.52
		.040 (.102)	85.12	85.16	85.22
		.110 (.279)	102.26	102.33	Not TM
		.355 (.901)	Not Rec	Not Rec	N.T.
67.5°	60°	0.040 (0.102)	83.03	83.10	83.18
		.160 (.406)	100.94	100.98	101.02
		.460 (1.169)	N.T.	N.T.	Not TM
		.511 (1.298)	Not Rec	Not Rec	N.T.
67.5°	180°	0.025 (0.064) (thru)	81.37	81.39	81.50
		.050 (.127)	90.13	90.20	90.18
		.209 (.533)	128.18	128.22	Not TM
		.310 (.787)	Not Rec	Not Rec	N.T.

[a](thru) indicates that the spring-wire sensor was located at its effective sensing depth in a hole drilled completely through the heat-shield material.

[b]N.T. indicates that the spring-wire sensor was unaffected by flight (i.e., not triggered); Not TM indicates that data signals applied to event recorder only (i.e., not telemetered); and Not Rec indicates that data signals applied to telemeter only (i.e., not recorded).

TABLE III.- THERMOCOUPLE DEPTHS

[3-element thermocouples]

Spacecraft station	Initial sensing depth of –		
	Element 1	Element 2	Element 3
45° Cone 1	Surface	0.096 in. (0.244 cm)	0.194 in. (0.493 cm)
Cone 2	Surface	.096 in. (0.244 cm)	.197 in. (0.500 cm)
Cylinder 1	Surface	.090 in. (0.229 cm)	.197 in. (0.500 cm)
	Surface	.099 in. (0.251 cm)	.201 in. (0.510 cm)

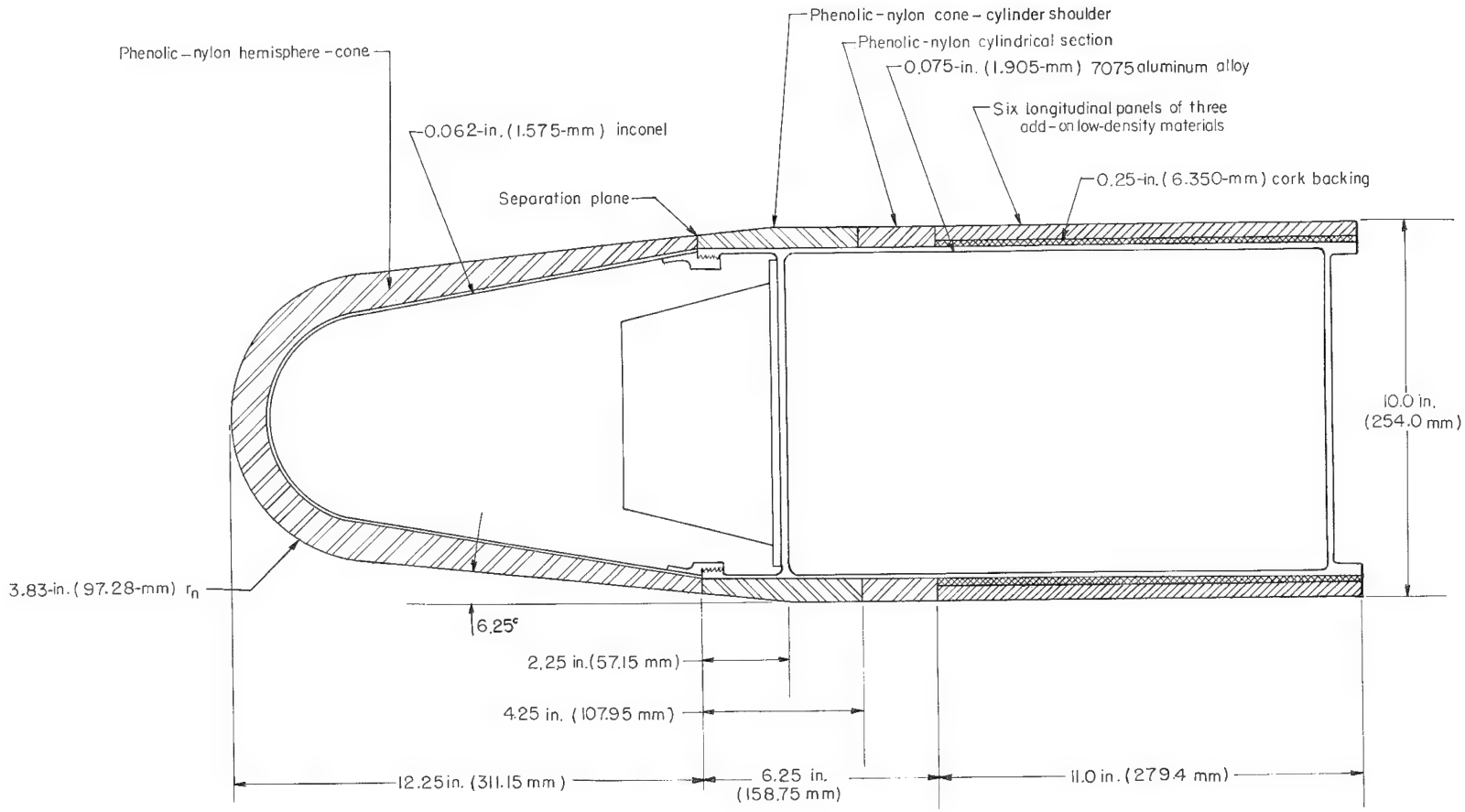

Figure 1.- Sketch of the spacecraft.

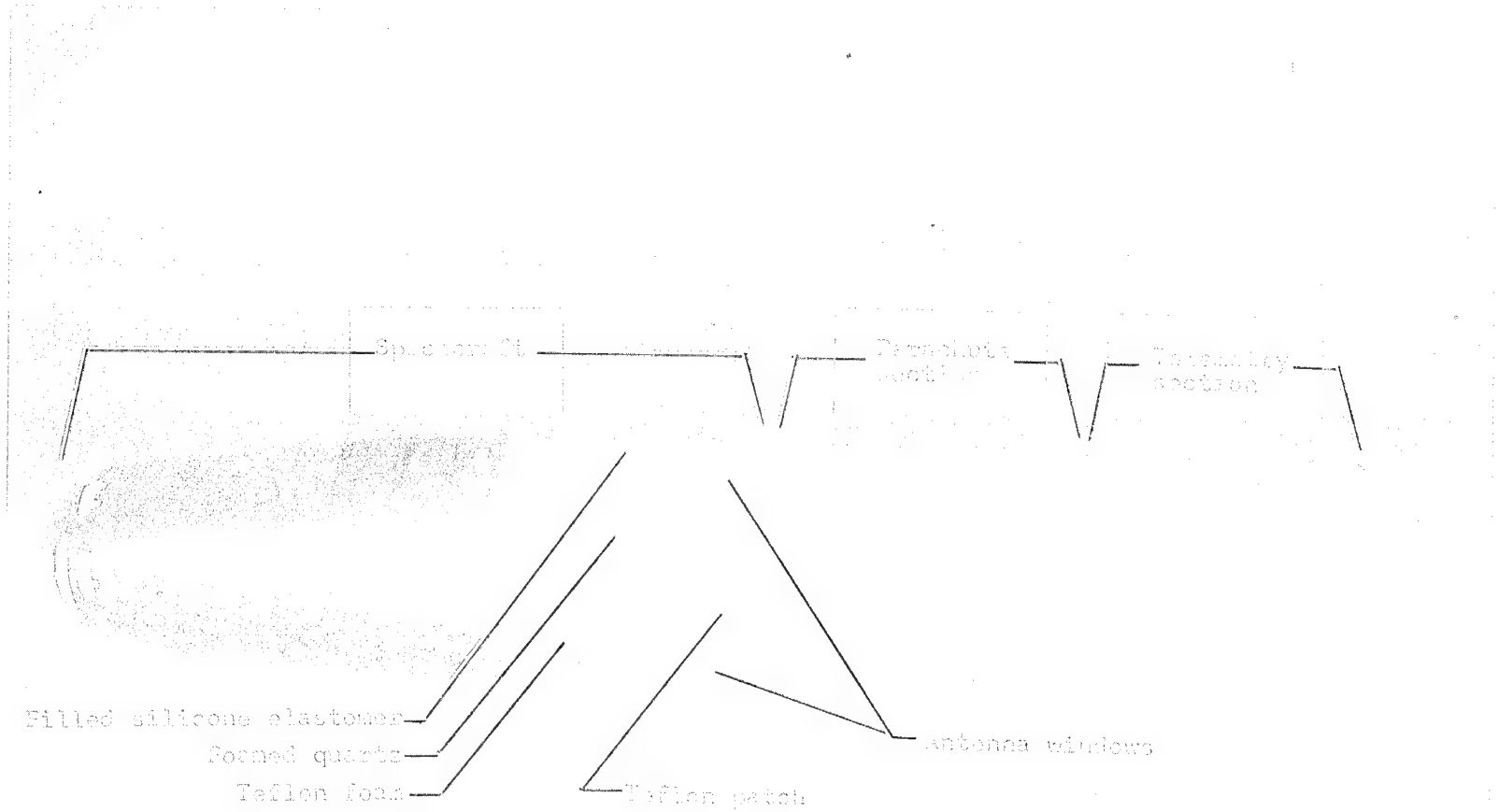

(a) Assembled.

L-68-5377

Figure 2.- Photograph of the spacecraft and the parachute and telemetry sections.

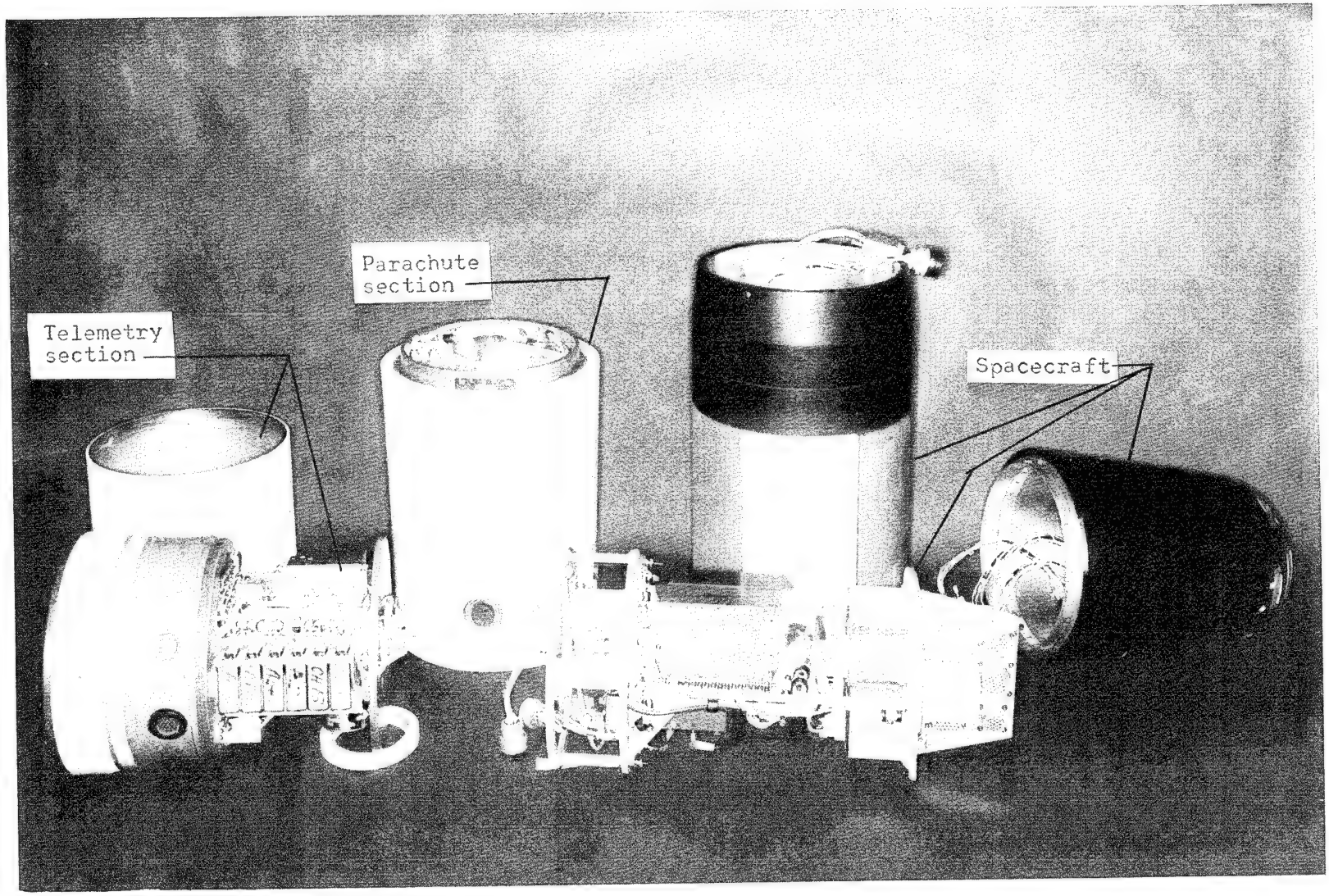

(b) Disassembled.

L-68-5376.1

Figure 2.- Concluded.

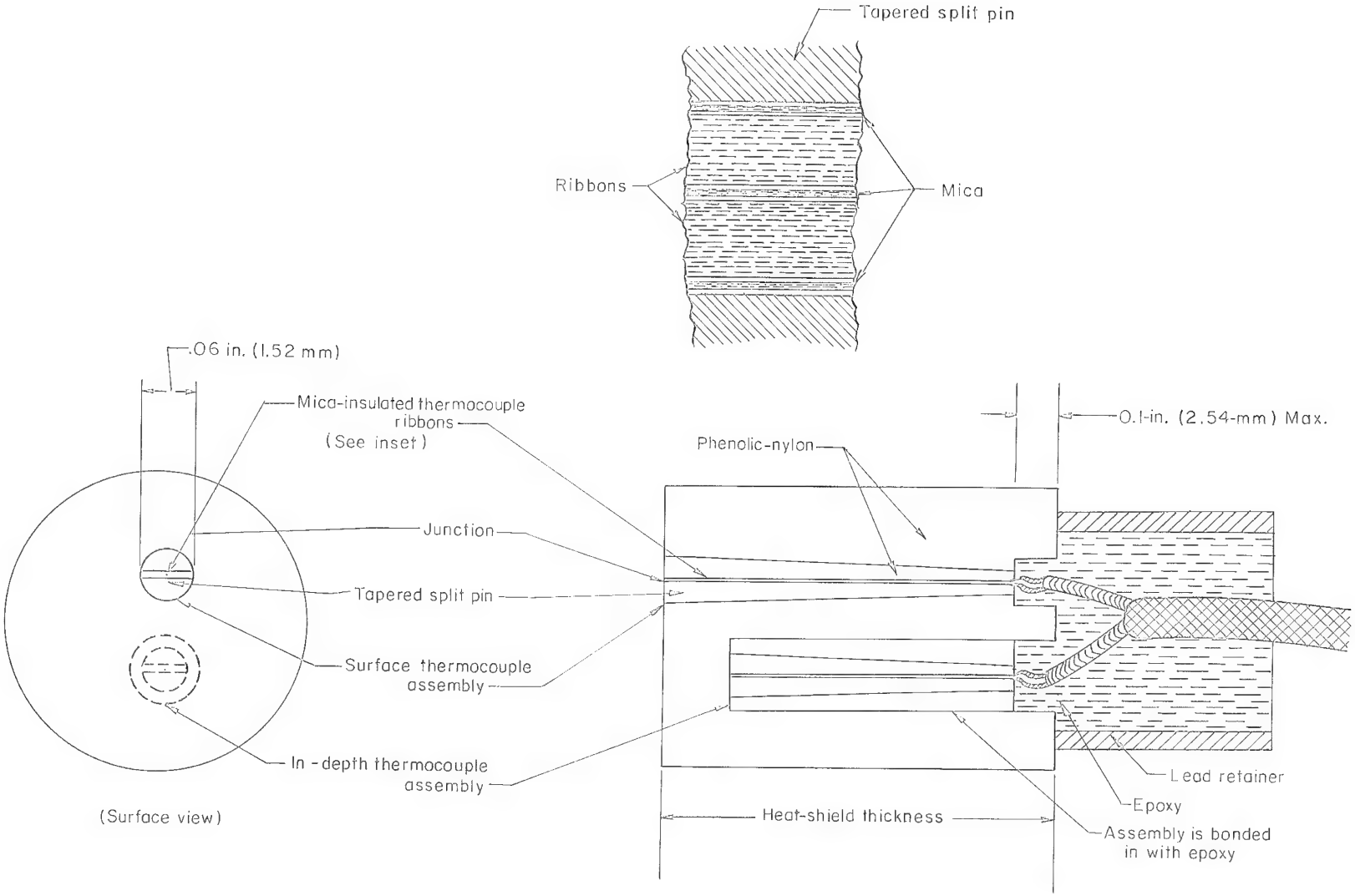

Figure 3.- Sketch of a typical thermocouple plug with one surface thermocouple assembly and one in-depth thermocouple assembly.

Figure 4.- Photograph of the spacecraft on the launch vehicle. L-68-4513

Figure 5.- Photograph of the recovered spacecraft.

L-68-4515

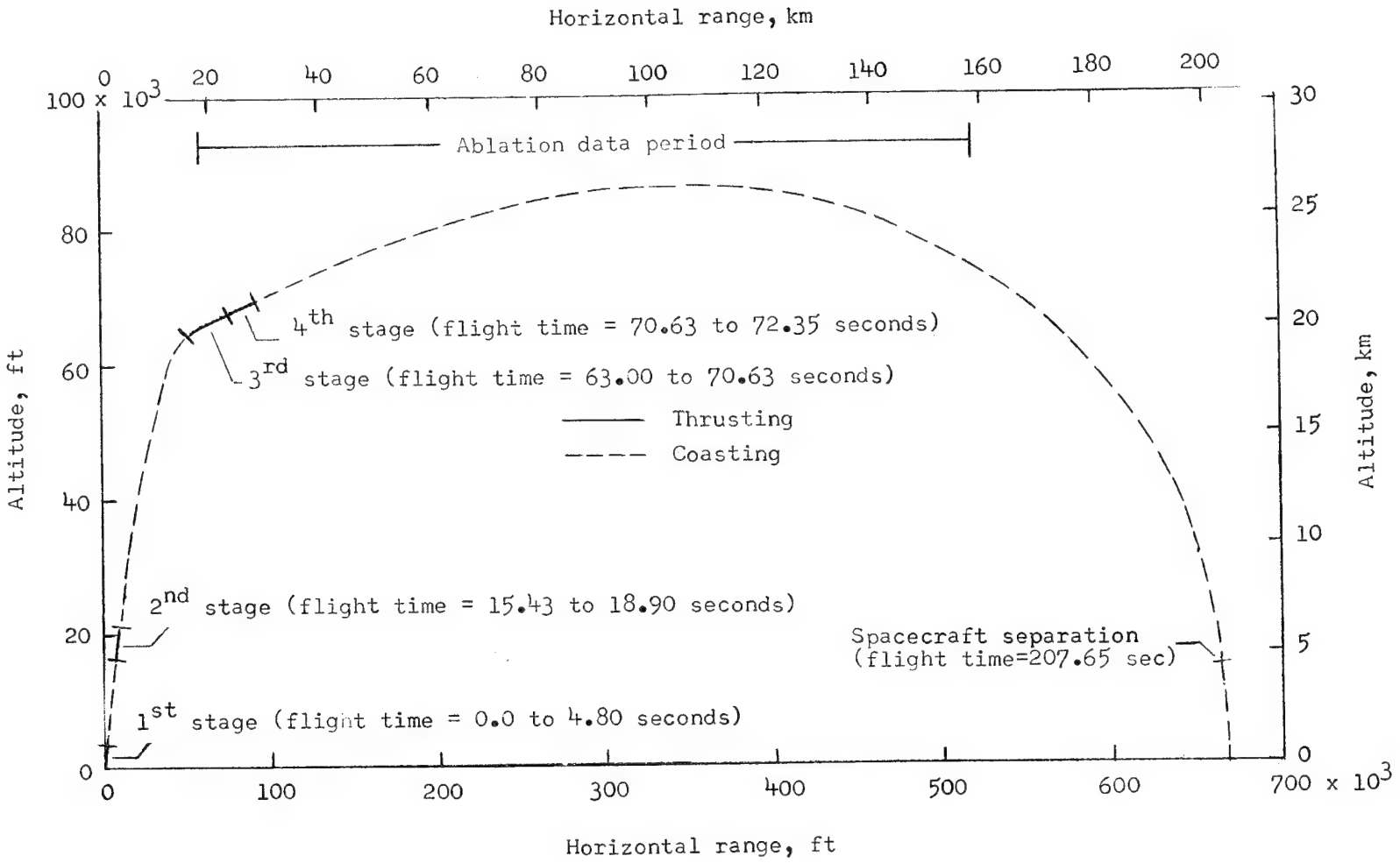

Figure 6.- Flight trajectory and sequence of events.

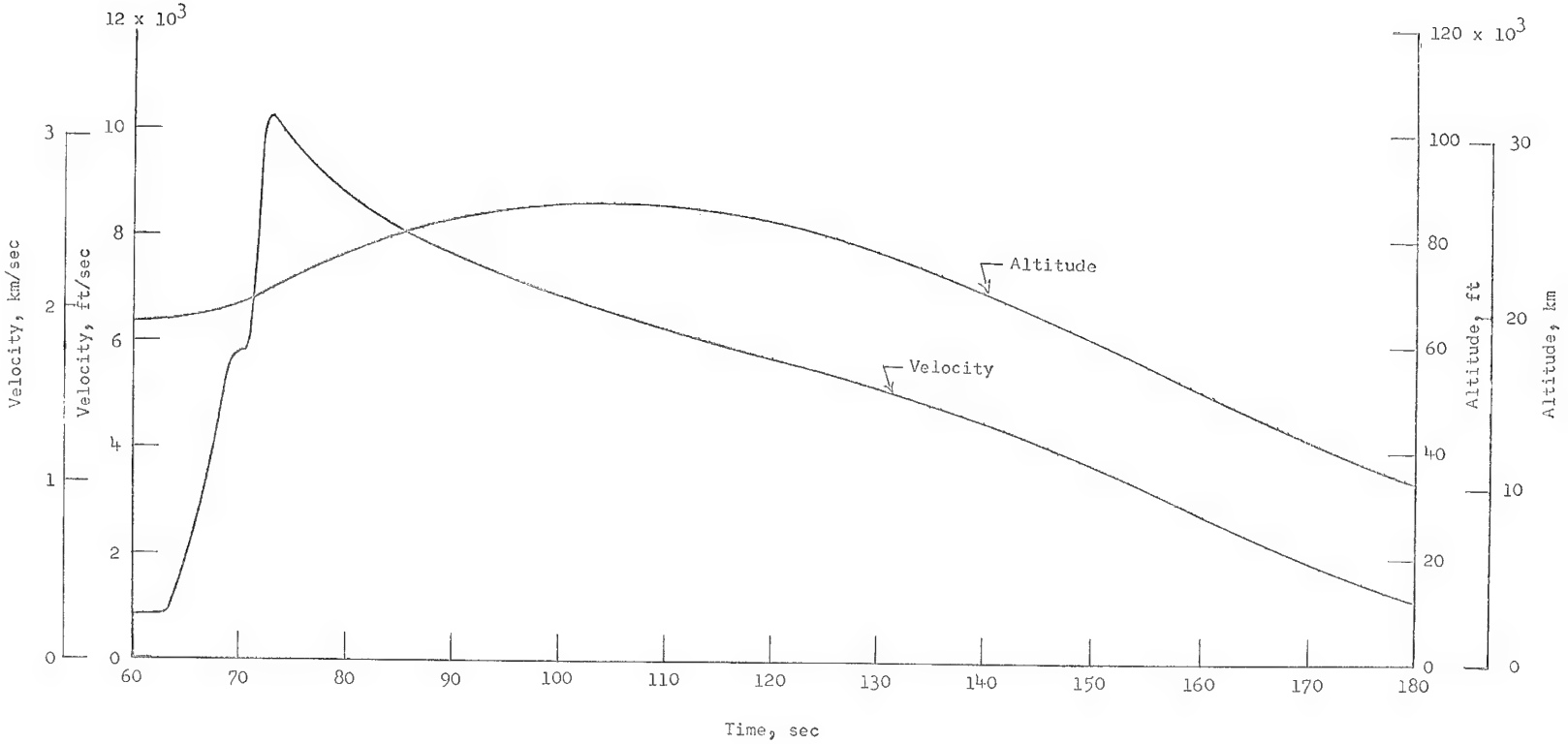

Figure 7.- Time histories of altitude and velocity.

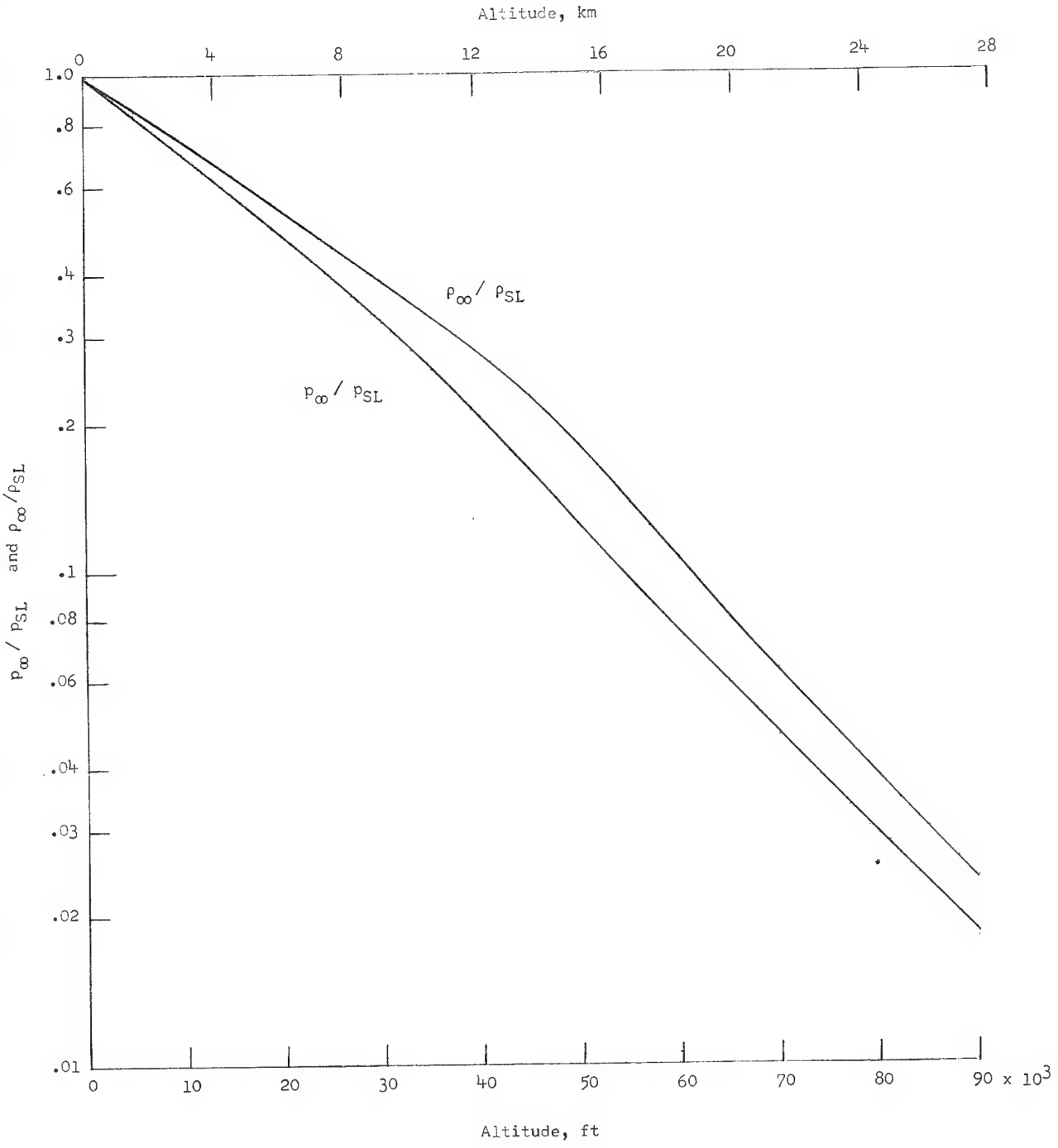

(a) Variation of nondimensional measured pressure and of nondimensional computed density with altitude.

Figure 8.- Atmospheric data.

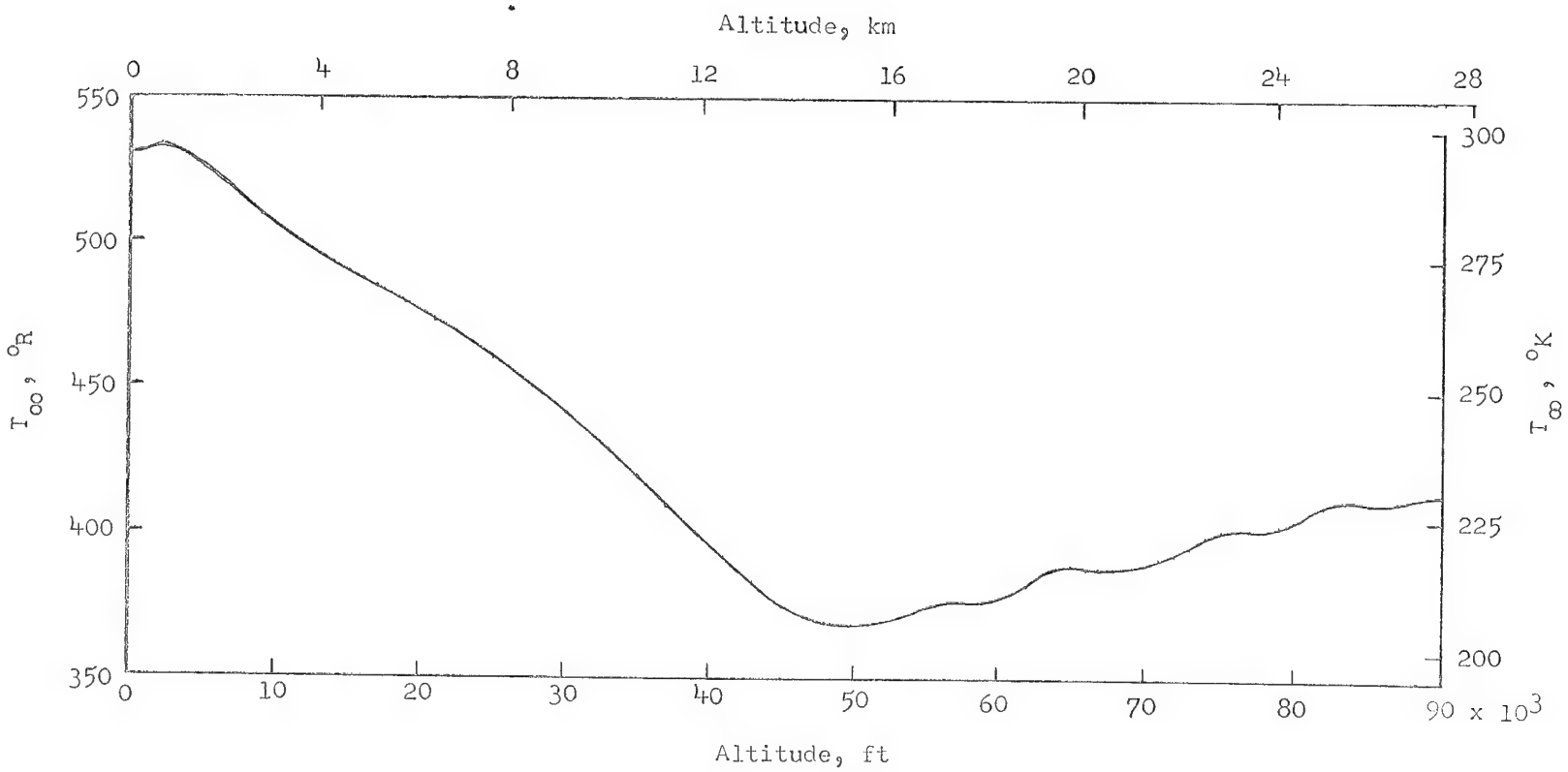

(b) Variation of measured temperature with altitude.

Figure 8.- Concluded.

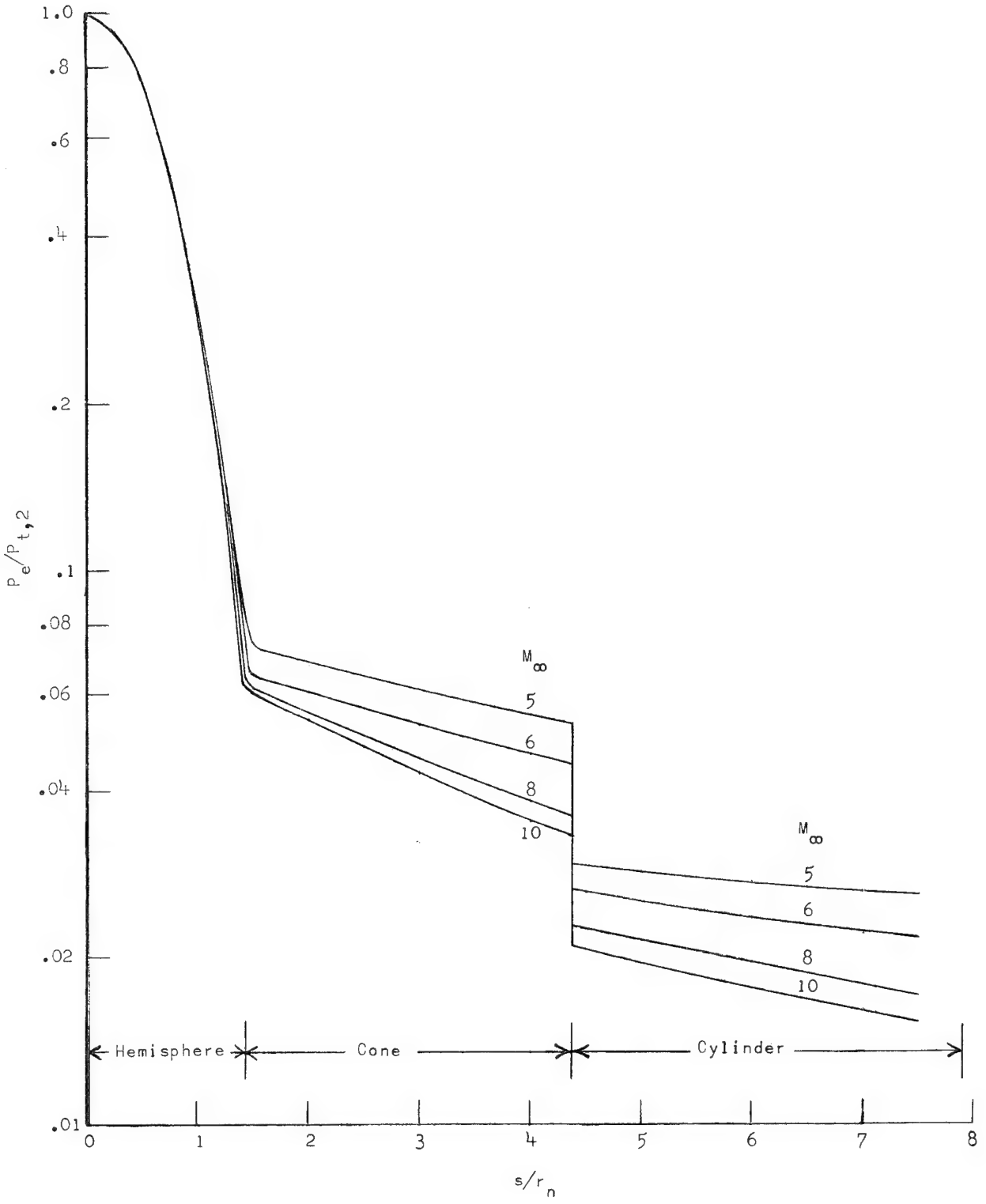

Figure 9.- Computed pressure distributions over the spacecraft.

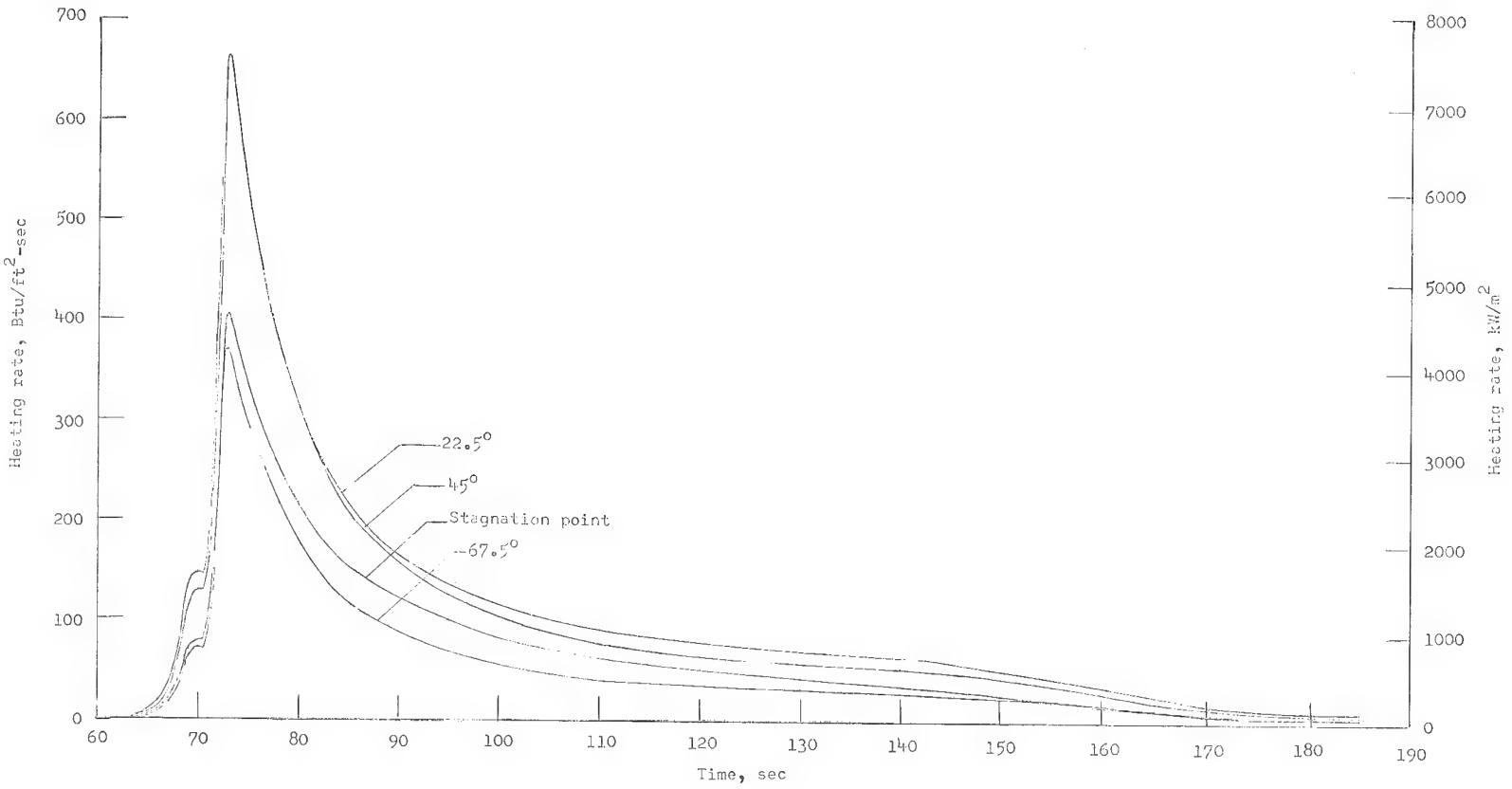

(a) Stations on the hemisphere (turbulent flow).

Figure 10.- Computed cold-wall heating rates.

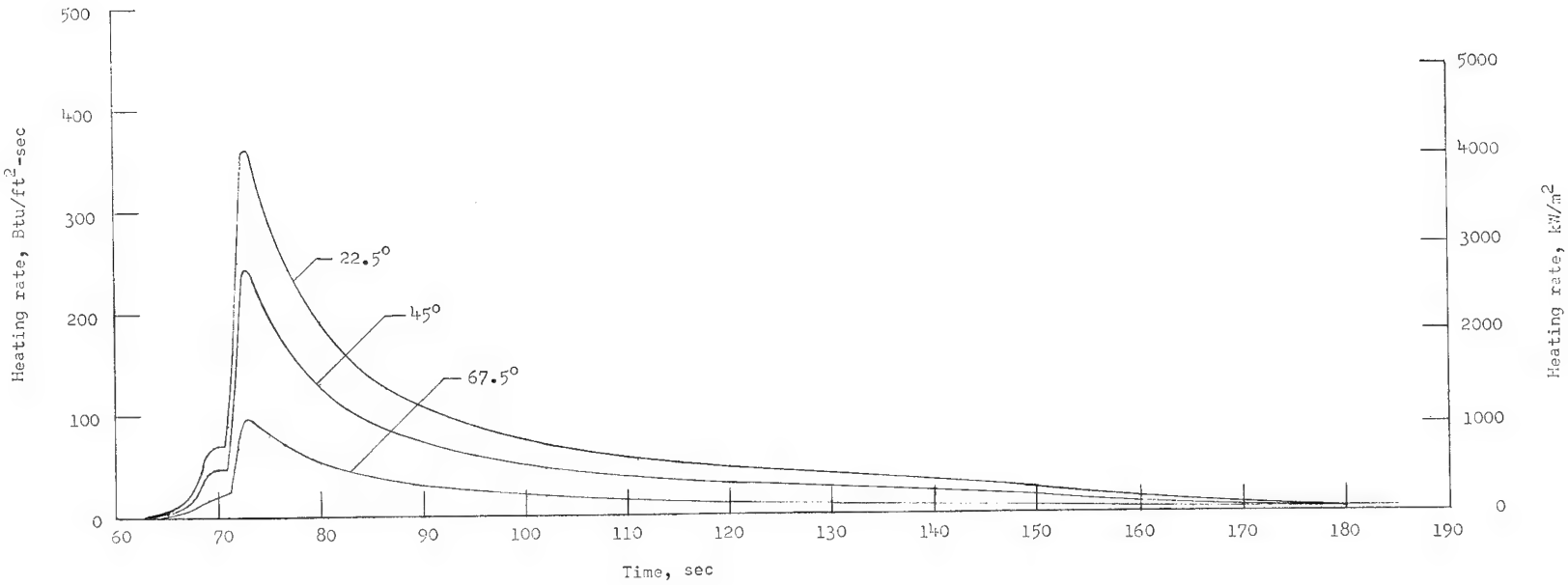

(b) Stations on the hemisphere (laminar flow).

Figure 10.- Continued.

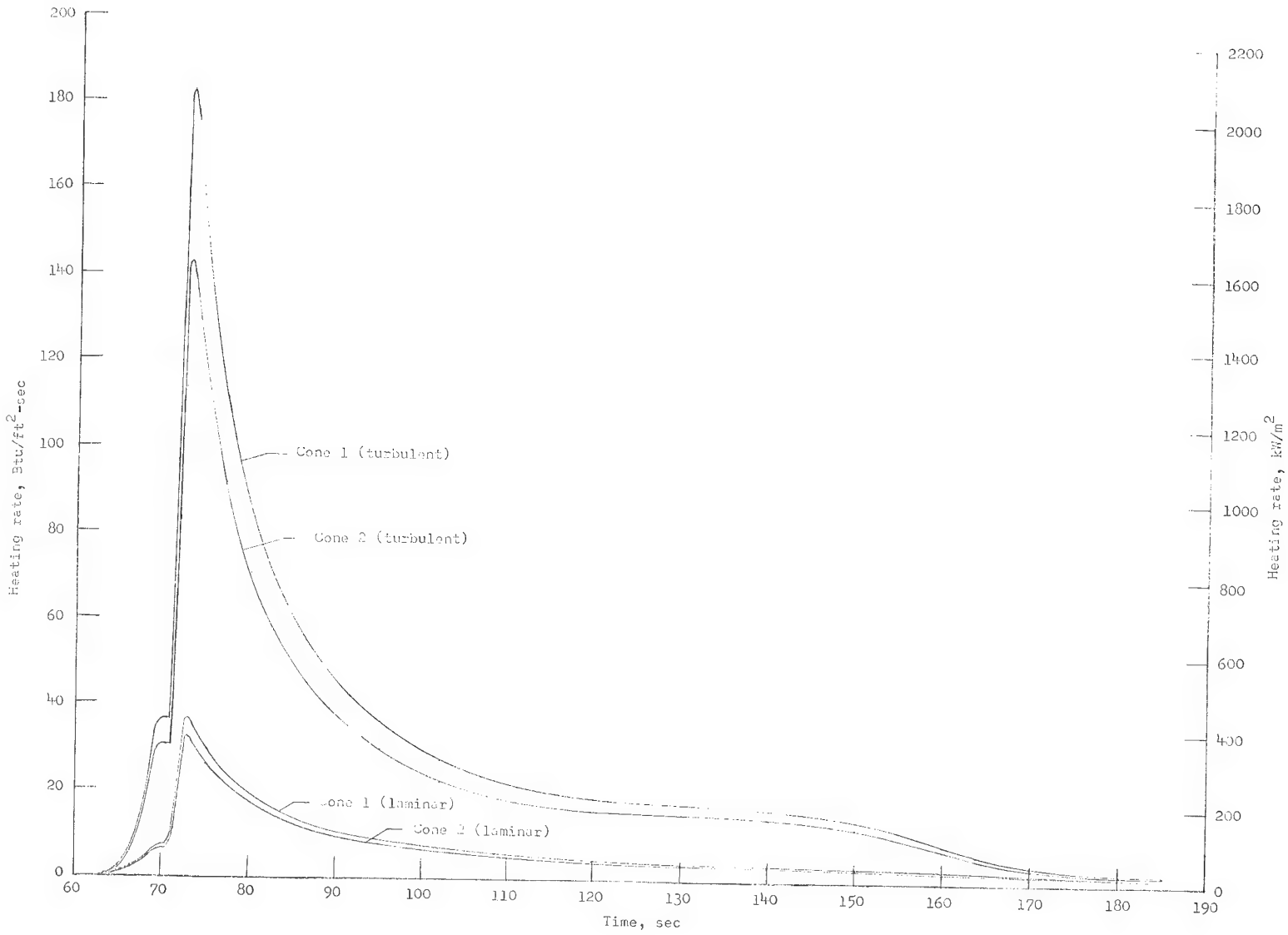

(c) Stations on the cone.

Figure 10.- Continued.

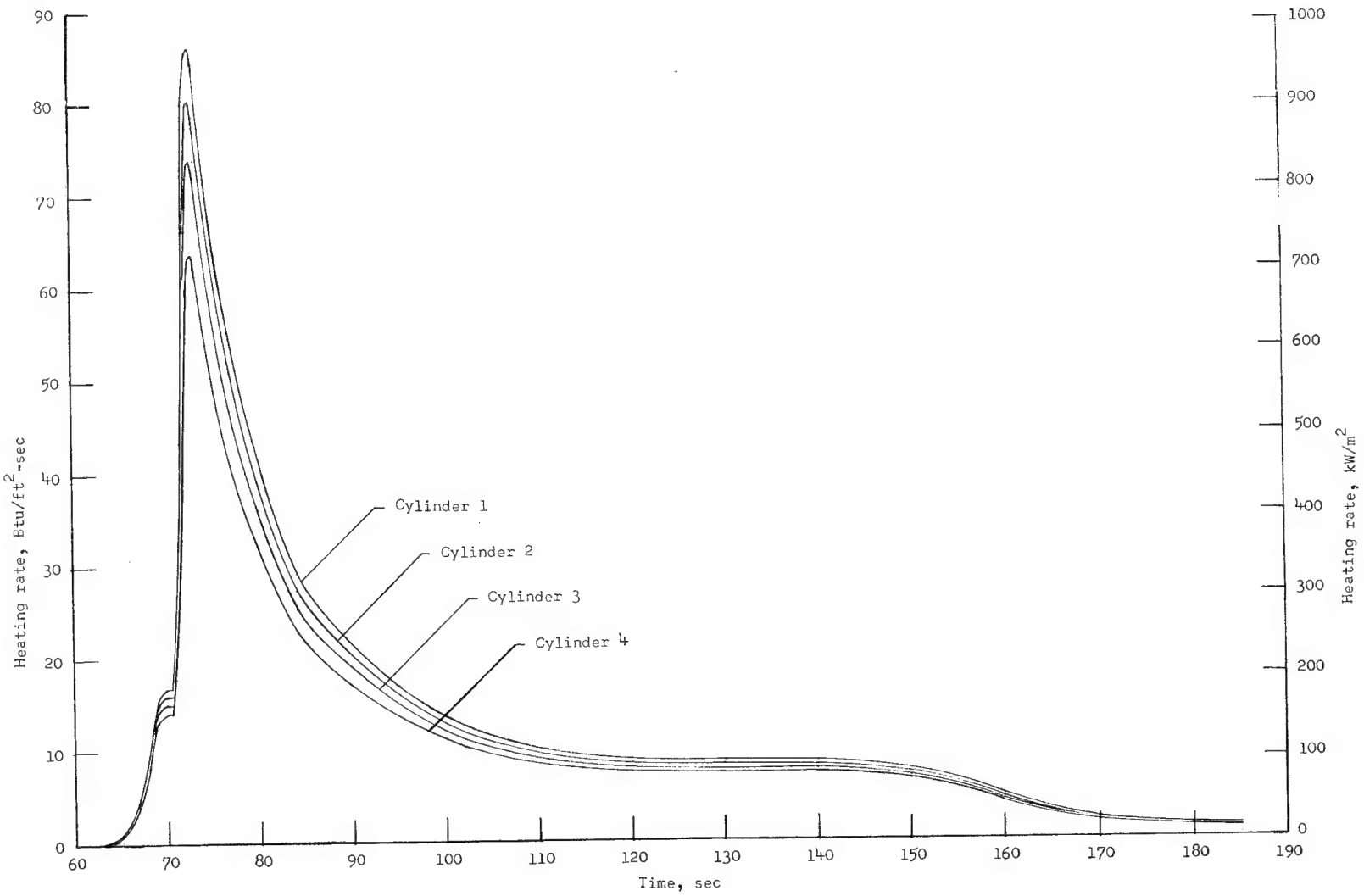

(d) Stations on the cylinder (turbulent flow).

Figure 10.- Continued.

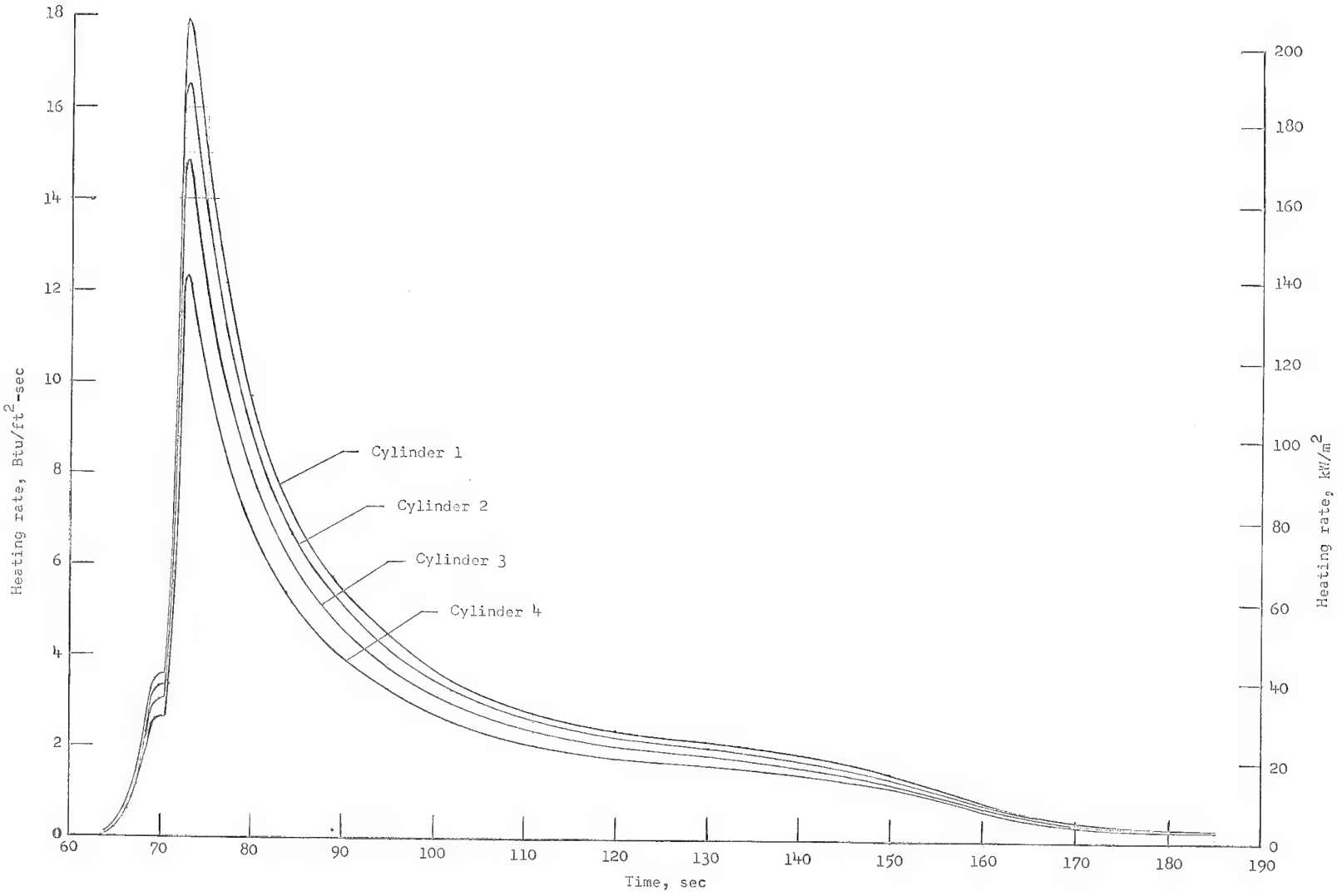

(e) Stations on the cylinder (laminar flow).

Figure 10.- Concluded.

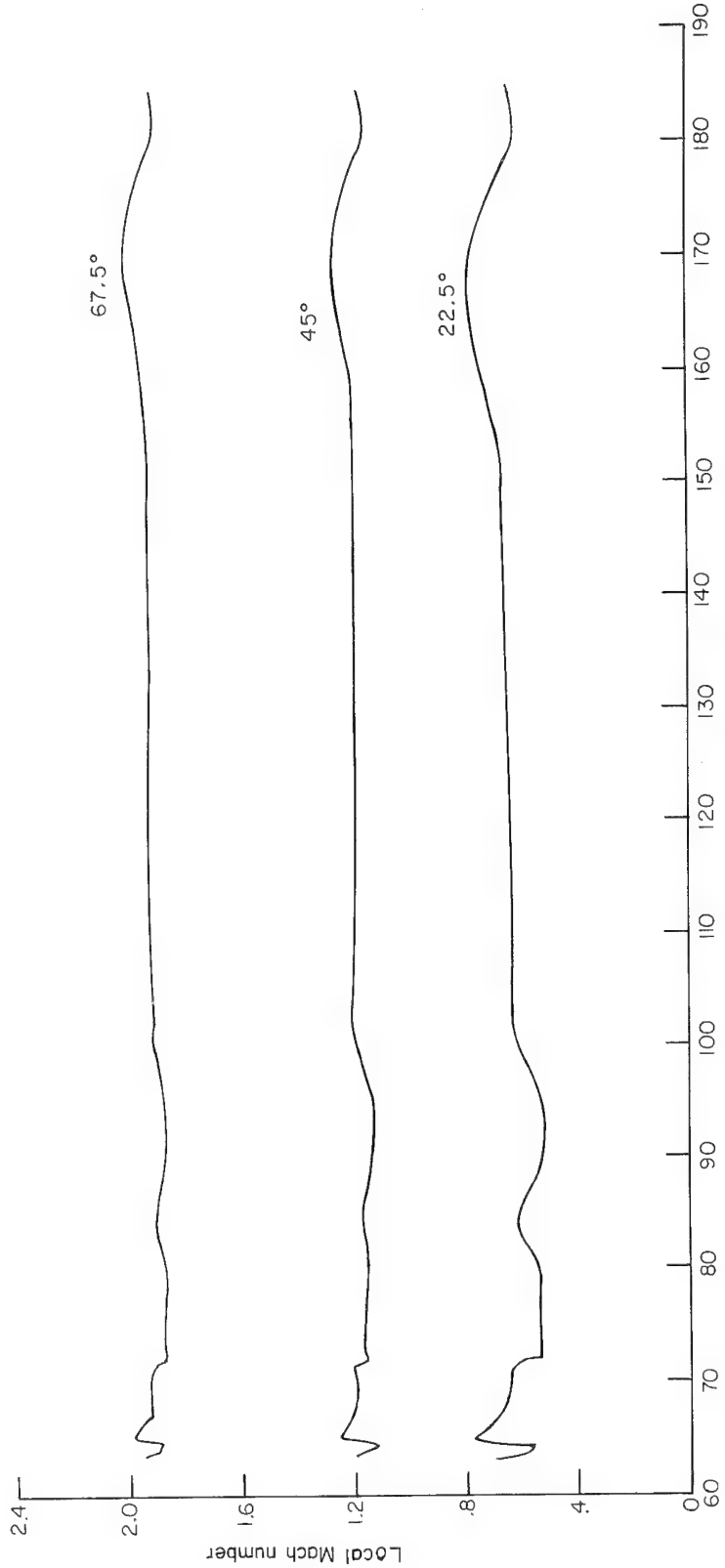

(a) Hemisphere.

Figure 11.- Computed local Mach number history.

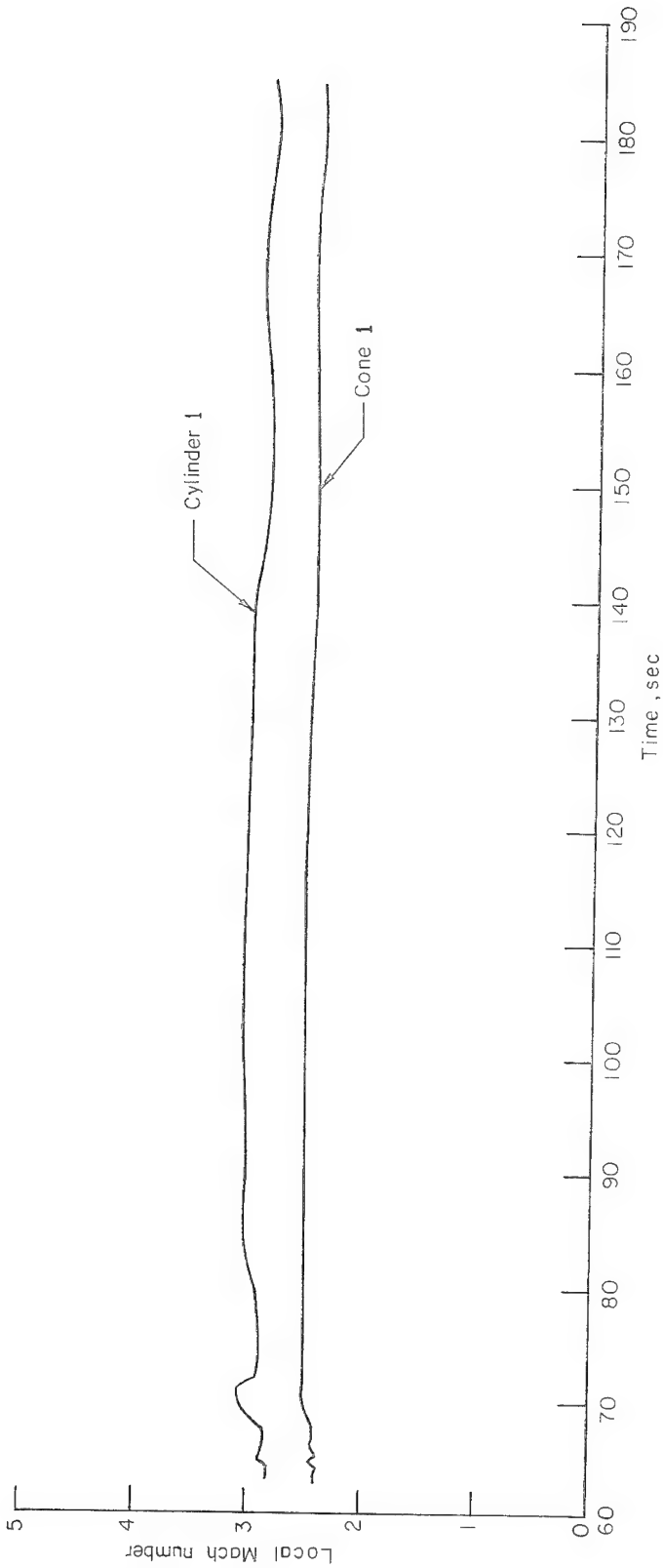

(b) Cone and cylinder.

Figure 11.- Concluded.

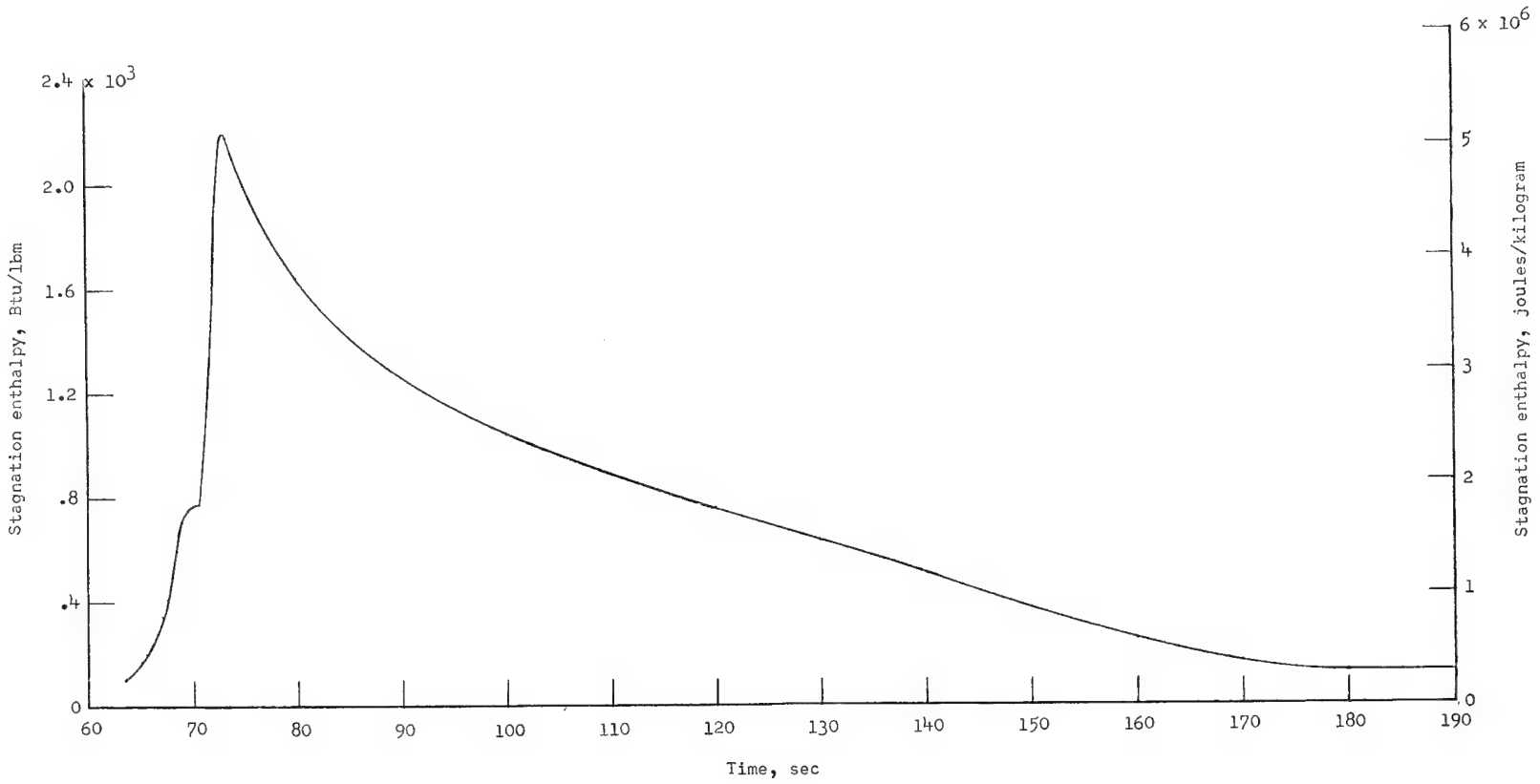

Figure 12.- Computed time history of stagnation enthalpy.

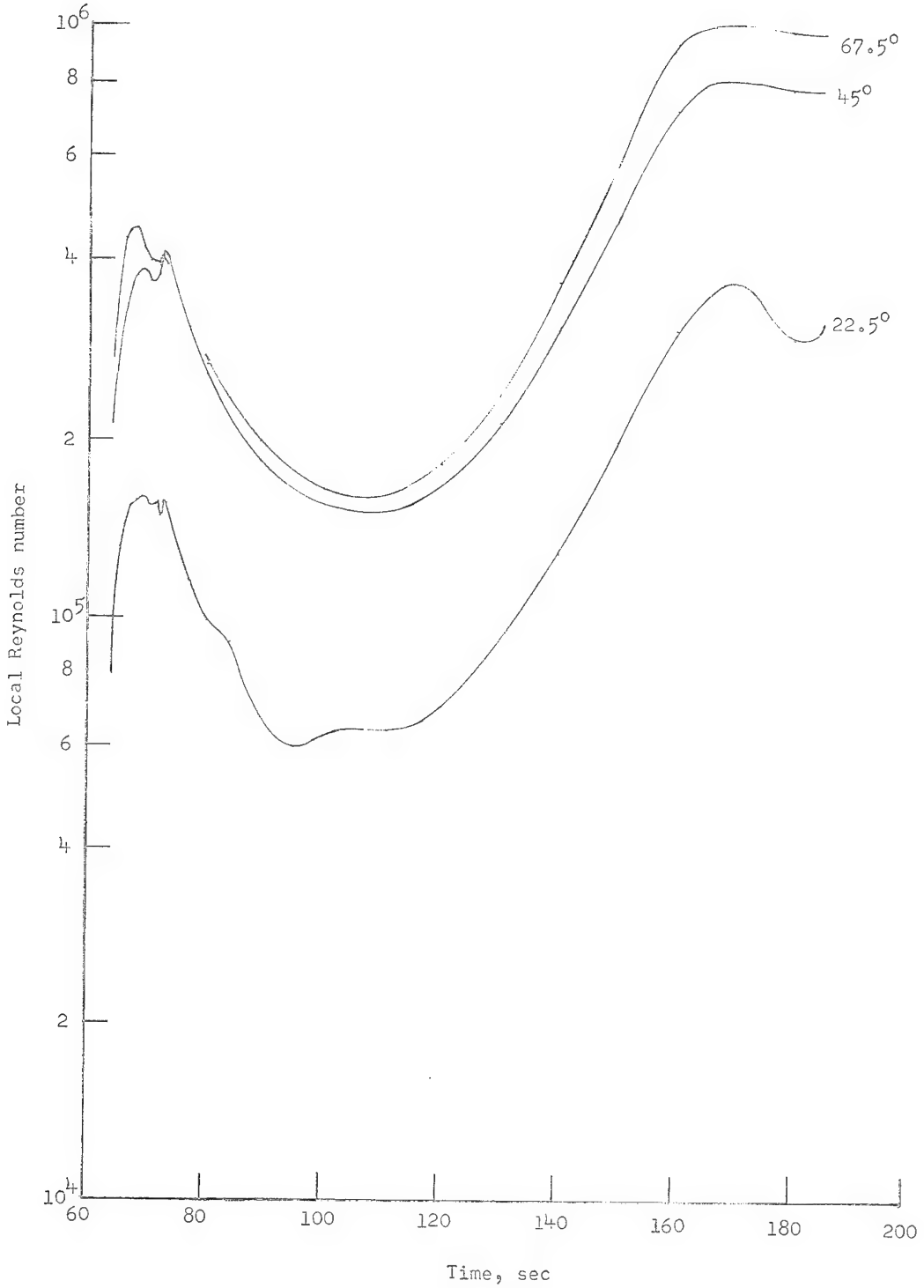

(a) Stations on the hemisphere.

Figure 13.- Computed time histories of local Reynolds numbers.

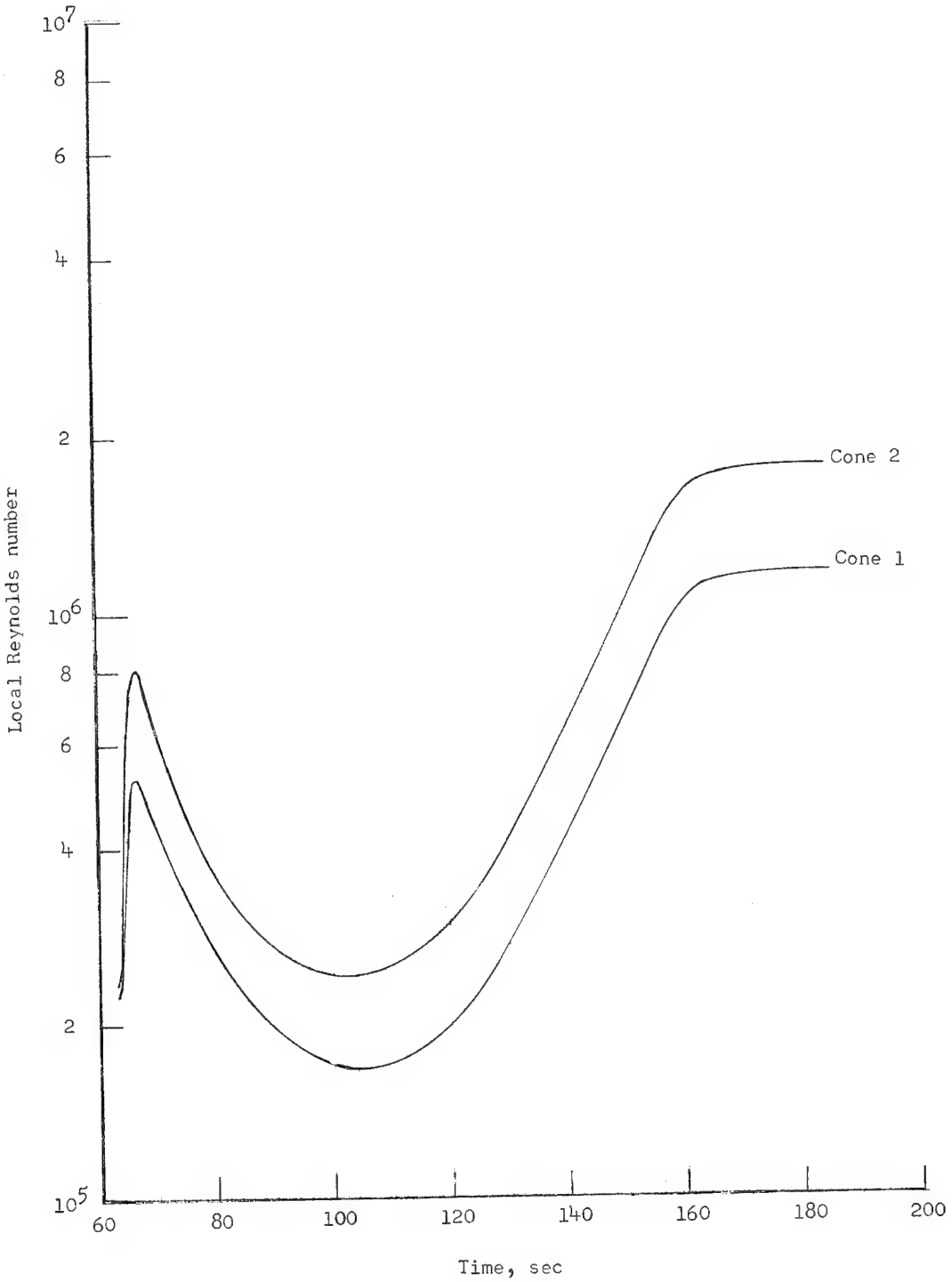

(b) Stations on the cone.

Figure 13.- Continued.

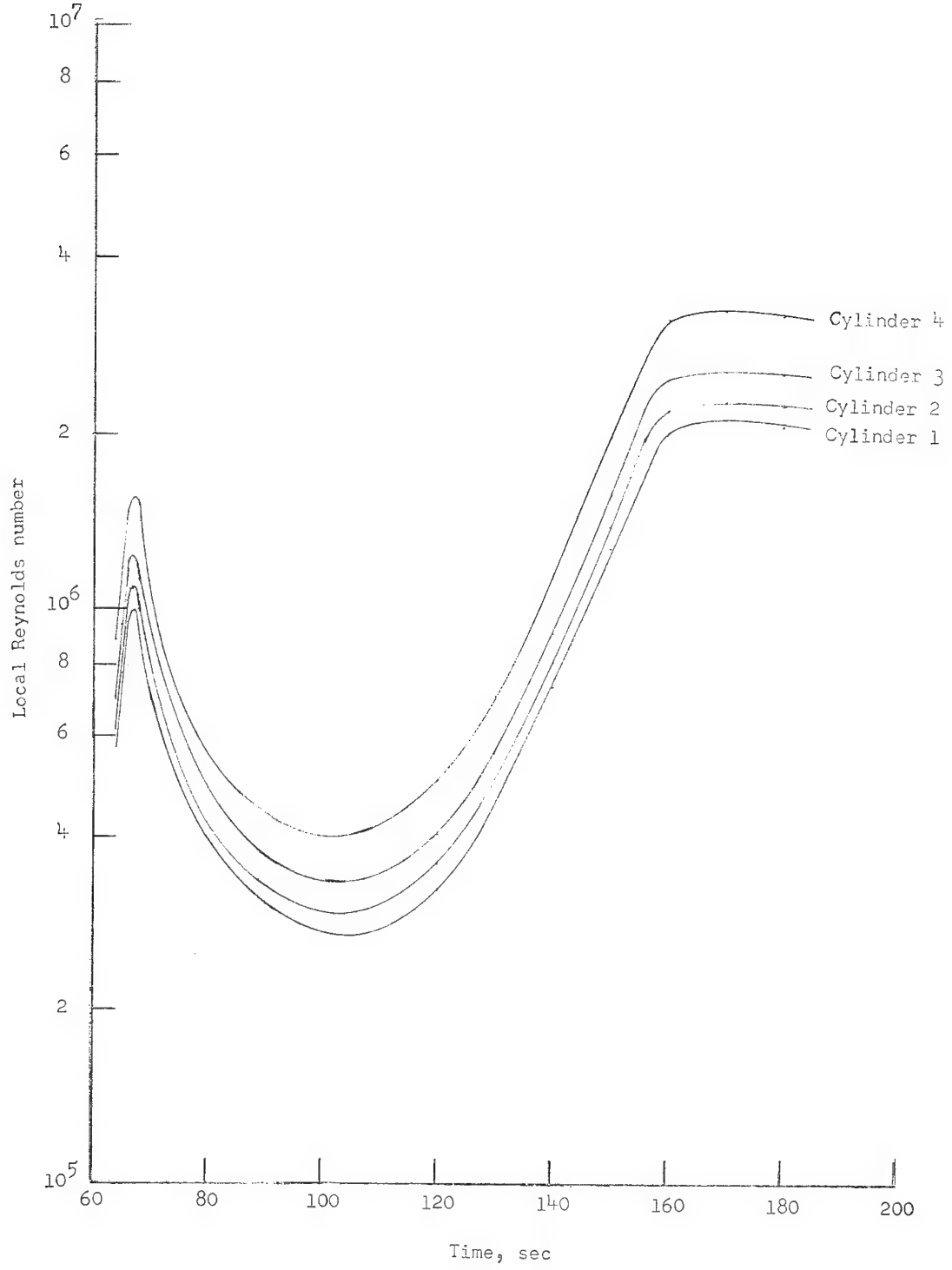

(c) Stations on the cylinder.

Figure 13.- Concluded.

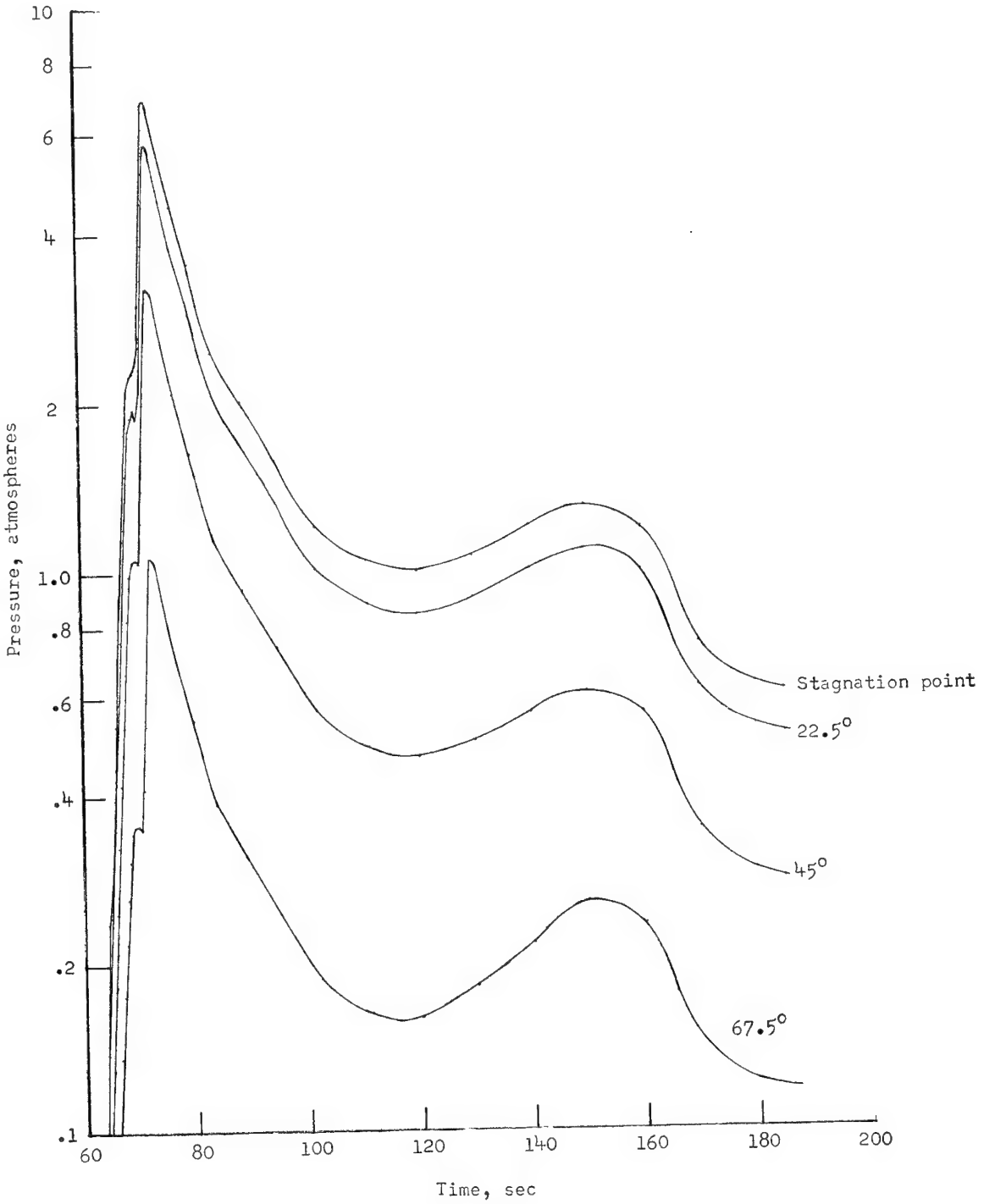

(a) Stations on the hemisphere.

Figure 14.- Computed time histories of local pressures.

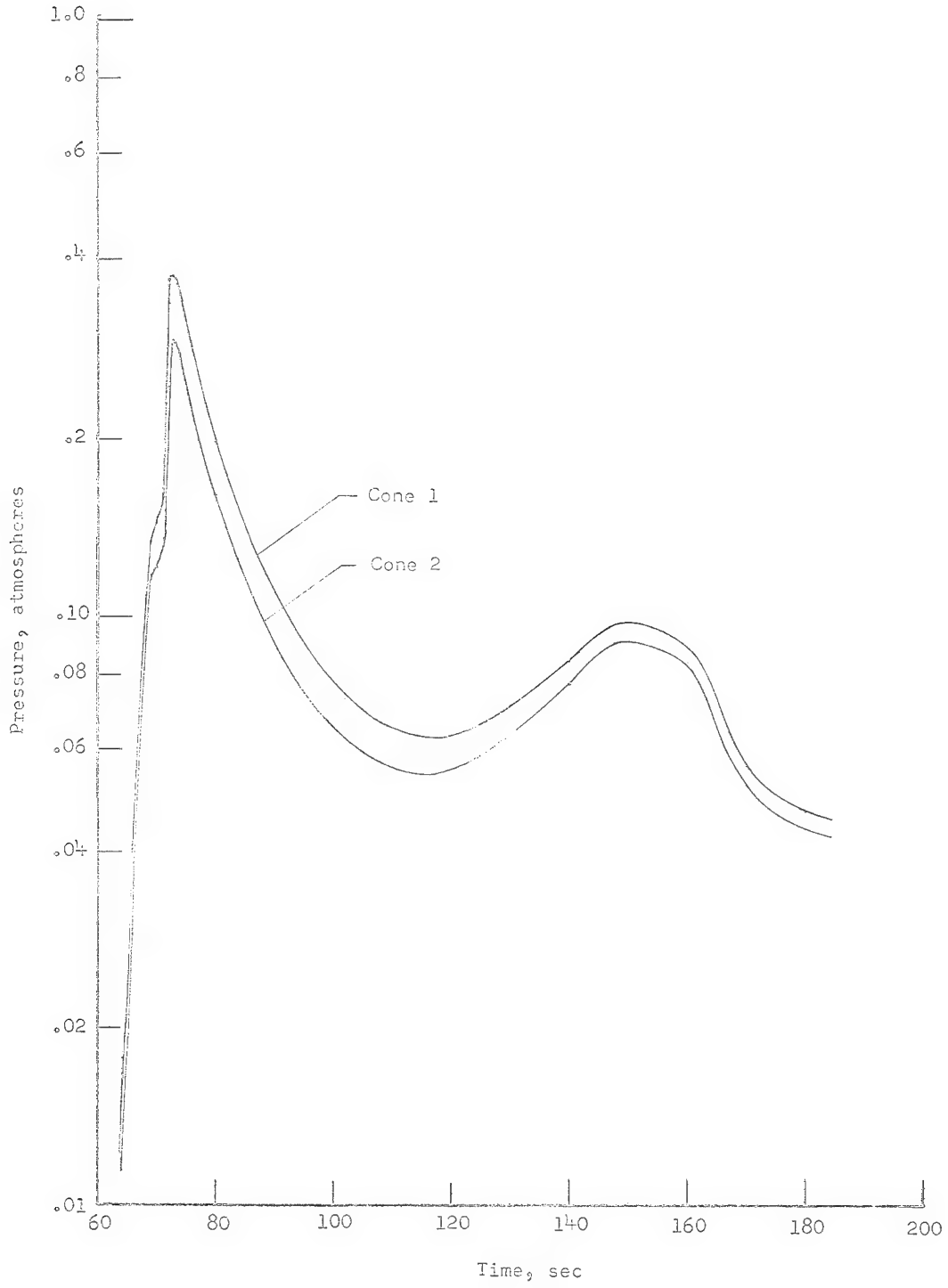

(b) Stations on the cone.

Figure 14.- Continued.

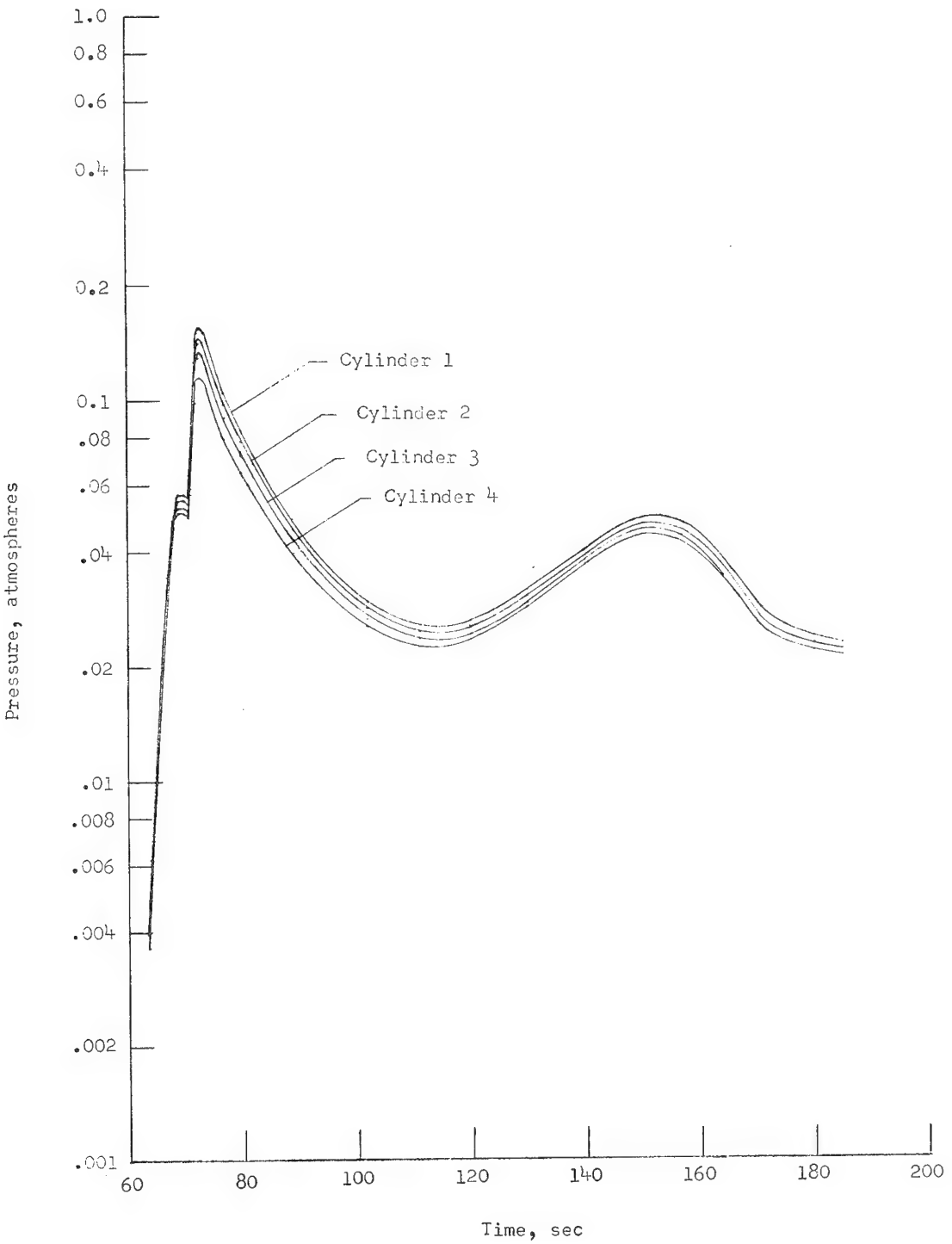

(c) Stations on the cylinder.

Figure 14.- Concluded.

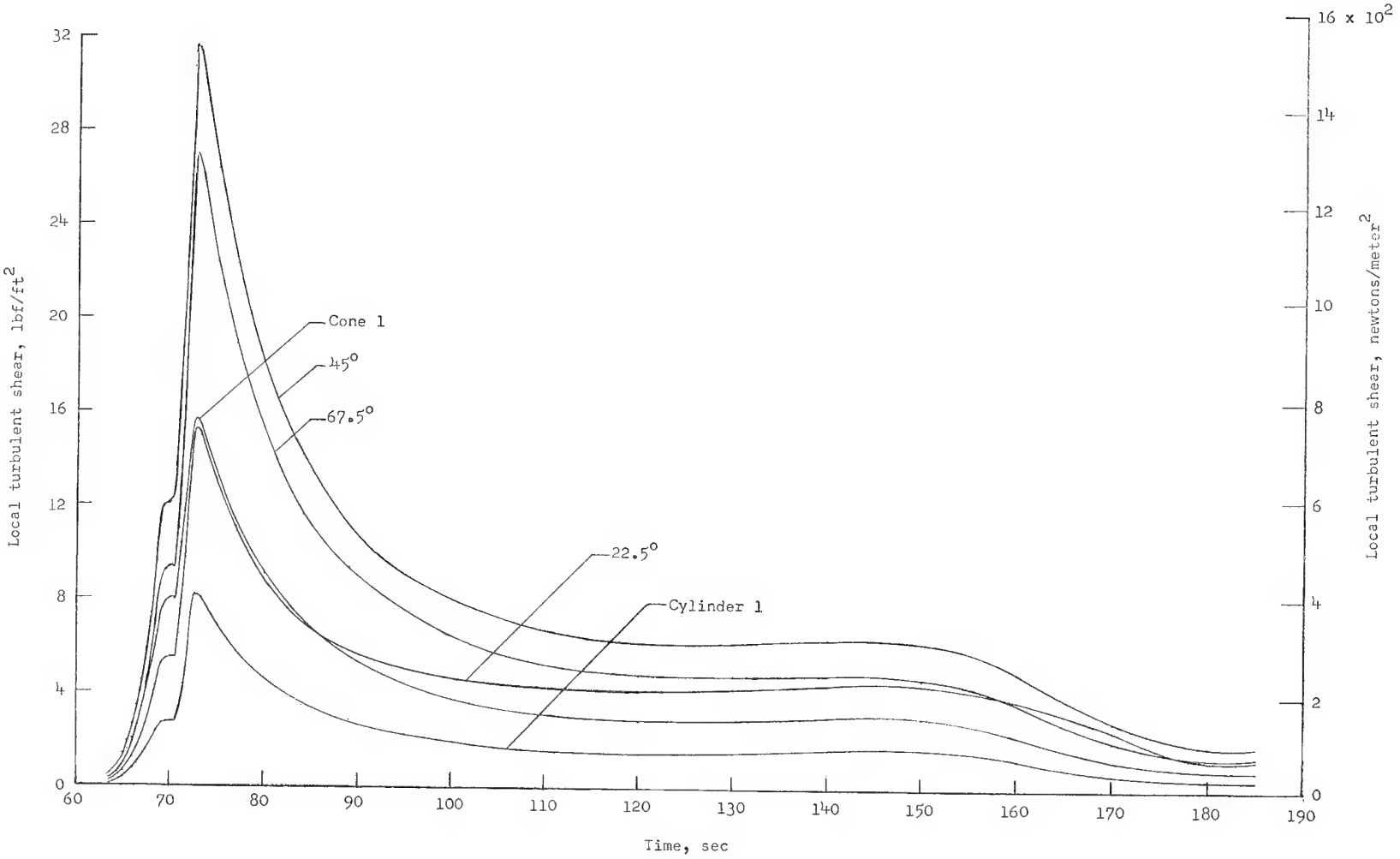

Figure 15.- Computed time histories of local turbulent shear.

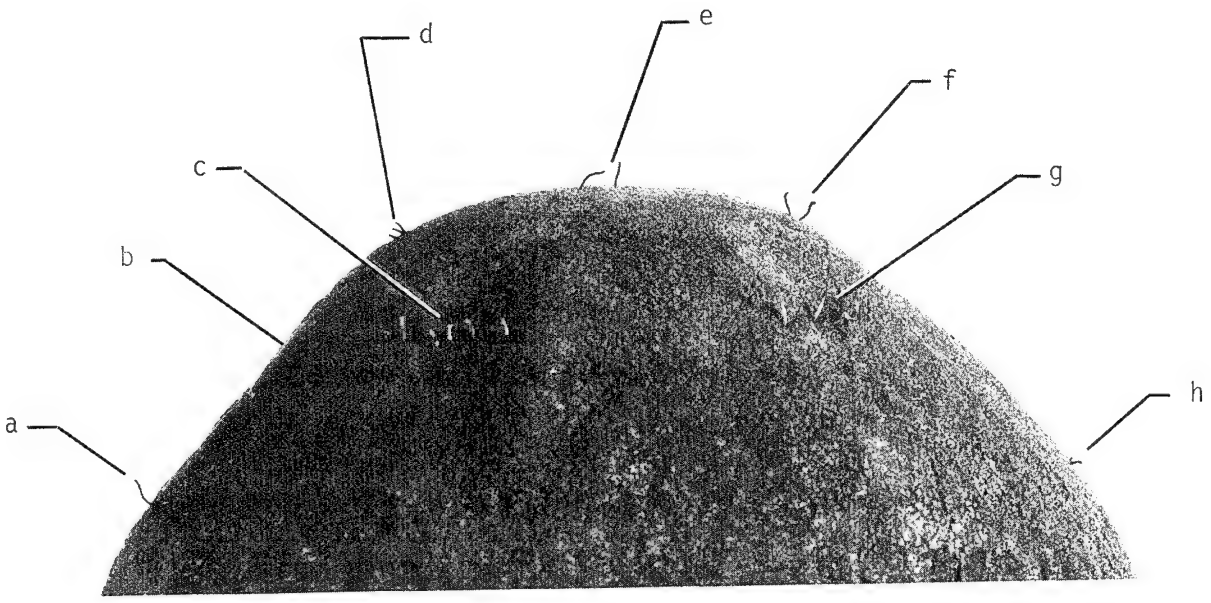

		Circumferential location, Ø	Spacecraft station
(a)	Dual ablation sensor	0°	67.5°
(b)	Thermocouple	0°	45.0°
(c)	Dual ablation sensor	300°	45.0°
(d)	Spring-wire sensor	0°	22.5°
(e)	Dual ablation sensor	0°	Stagnation point
(f)	Dual ablation sensor	180°	22.5°
(g)	Spring-wire sensor	240°	45.0°
(h)	Spring-wire sensor	180°	67.5°

Figure 16.- Closeup of the hemisphere. L-69-5390.1

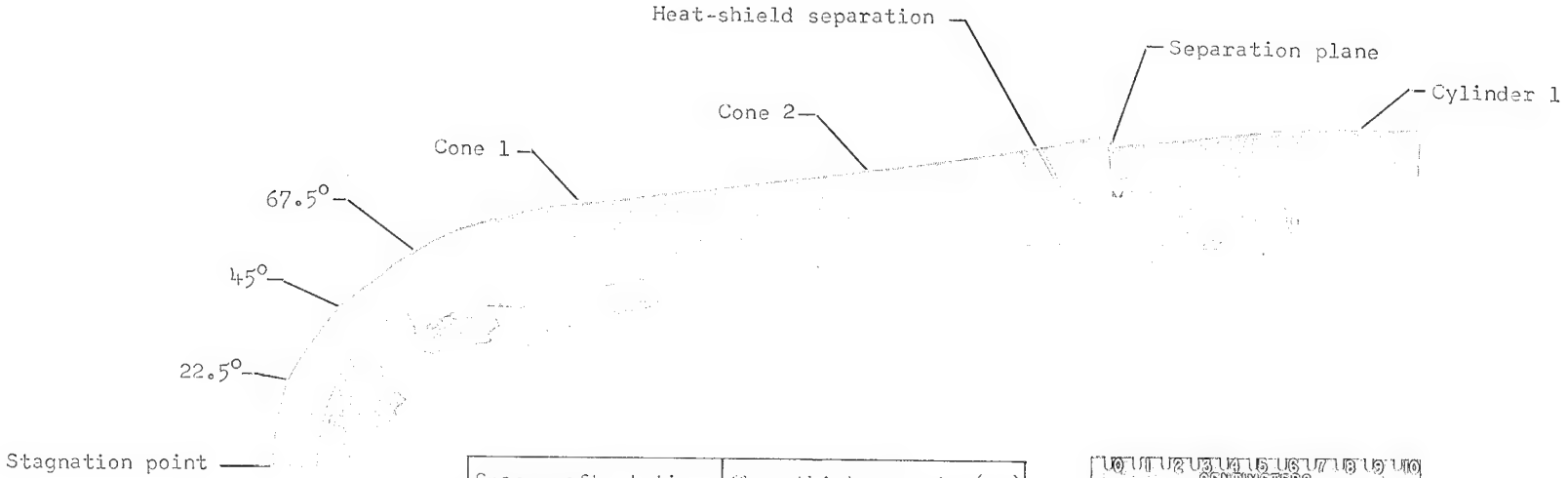

Spacecraft station	Char thickness, in.(mm)
Stagnation point	0.02 (0.51)
22.5°	.03 (.76)
45°	.03 (.76)
67.5°	.04 (1.02)
Cone 1	.05 (1.27)
Cone 2	.05 (1.27)
Cylinder 1	.03 (.76)

Figure 17.- Section of phenolic-nylon taken from the recovered spacecraft (60° circumferential location). L-69-4728.1

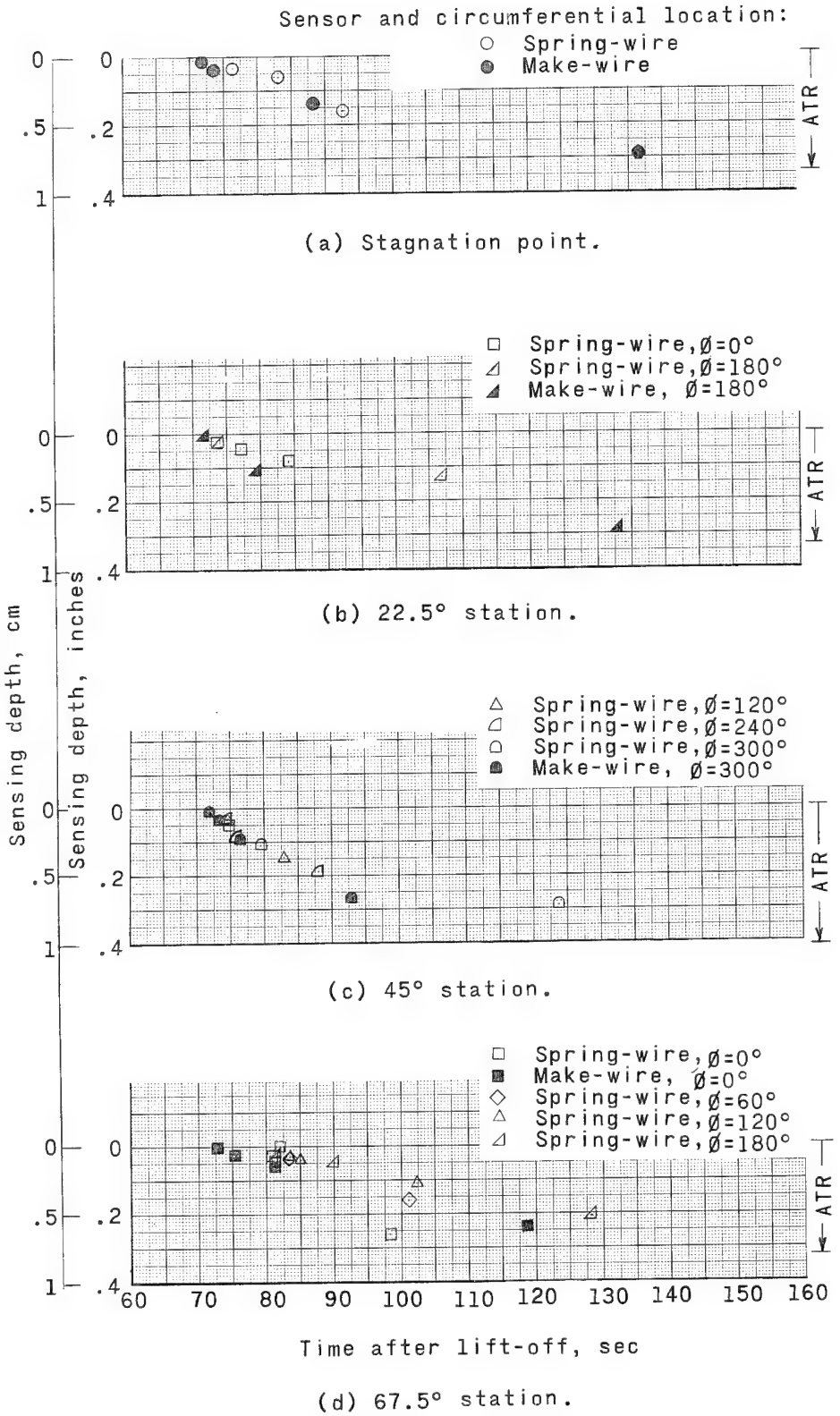

Figure 18.- Ablation data and average total recession (ATR).

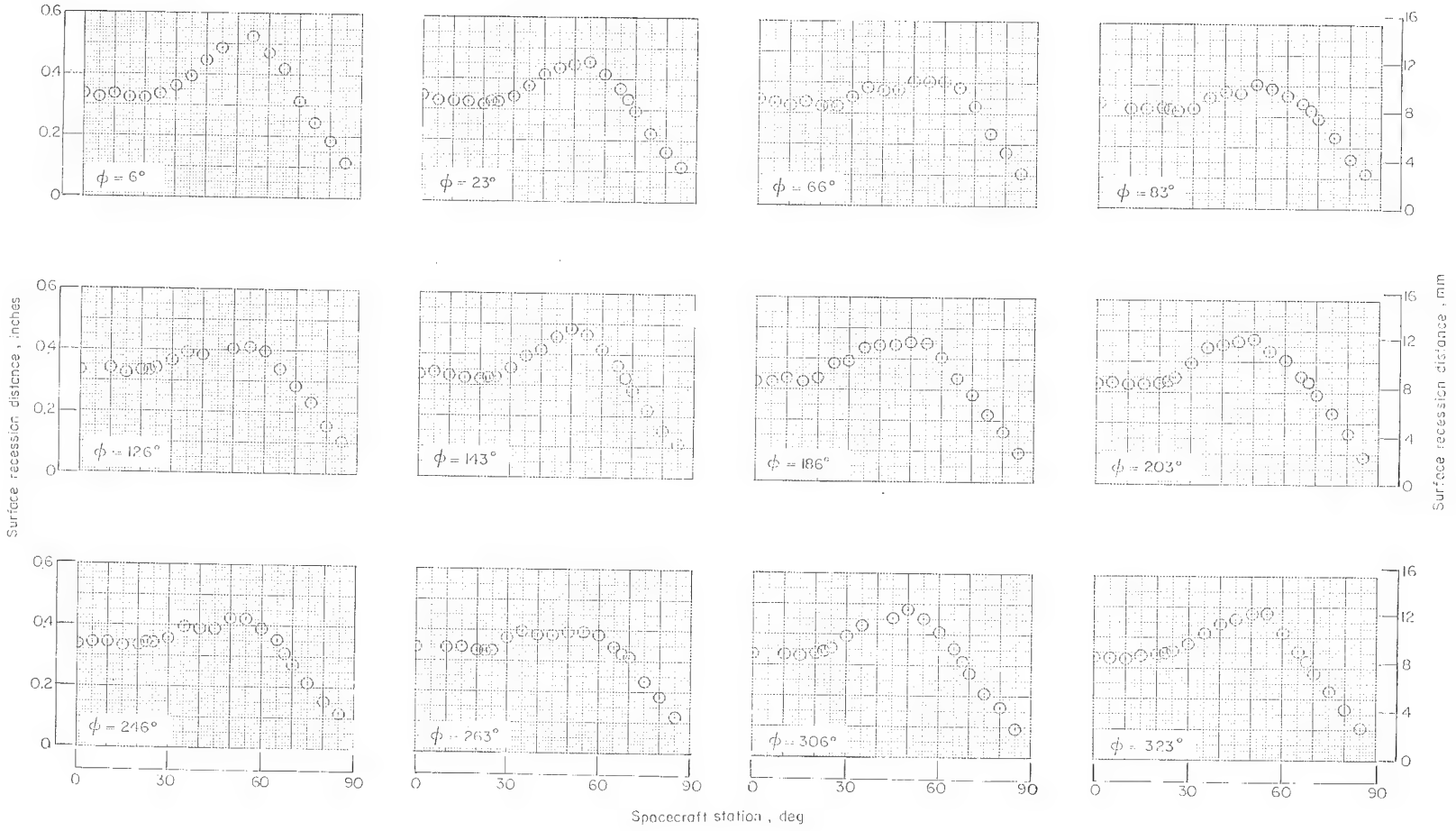

(a) Hemisphere.

Figure 19.- Recession or expansion distances of the spacecraft surface.

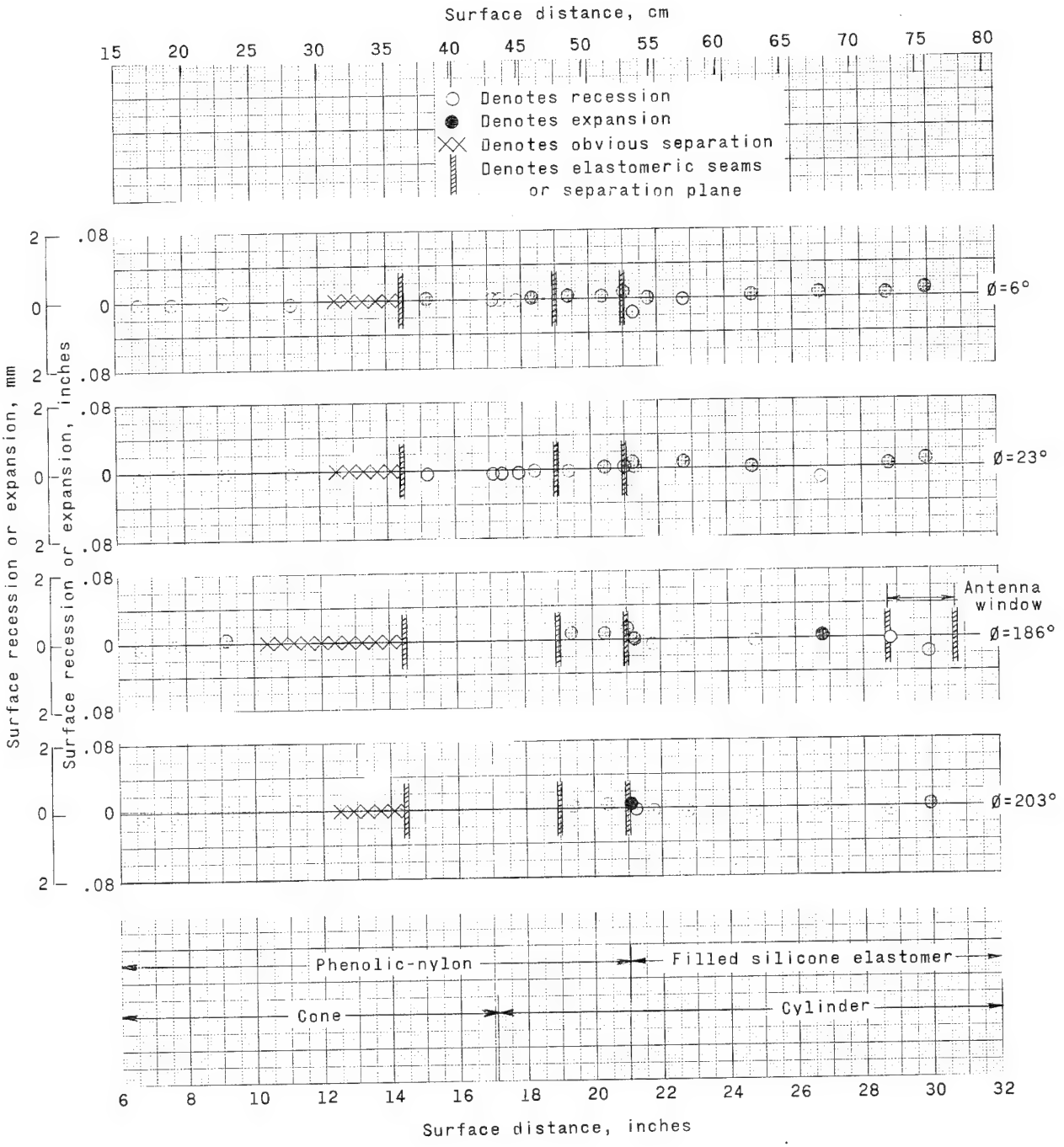

(b) Cone and cylinder (Φ = 6^0, 23^0, 186^0, and 203^0).

Figure 19.- Continued.

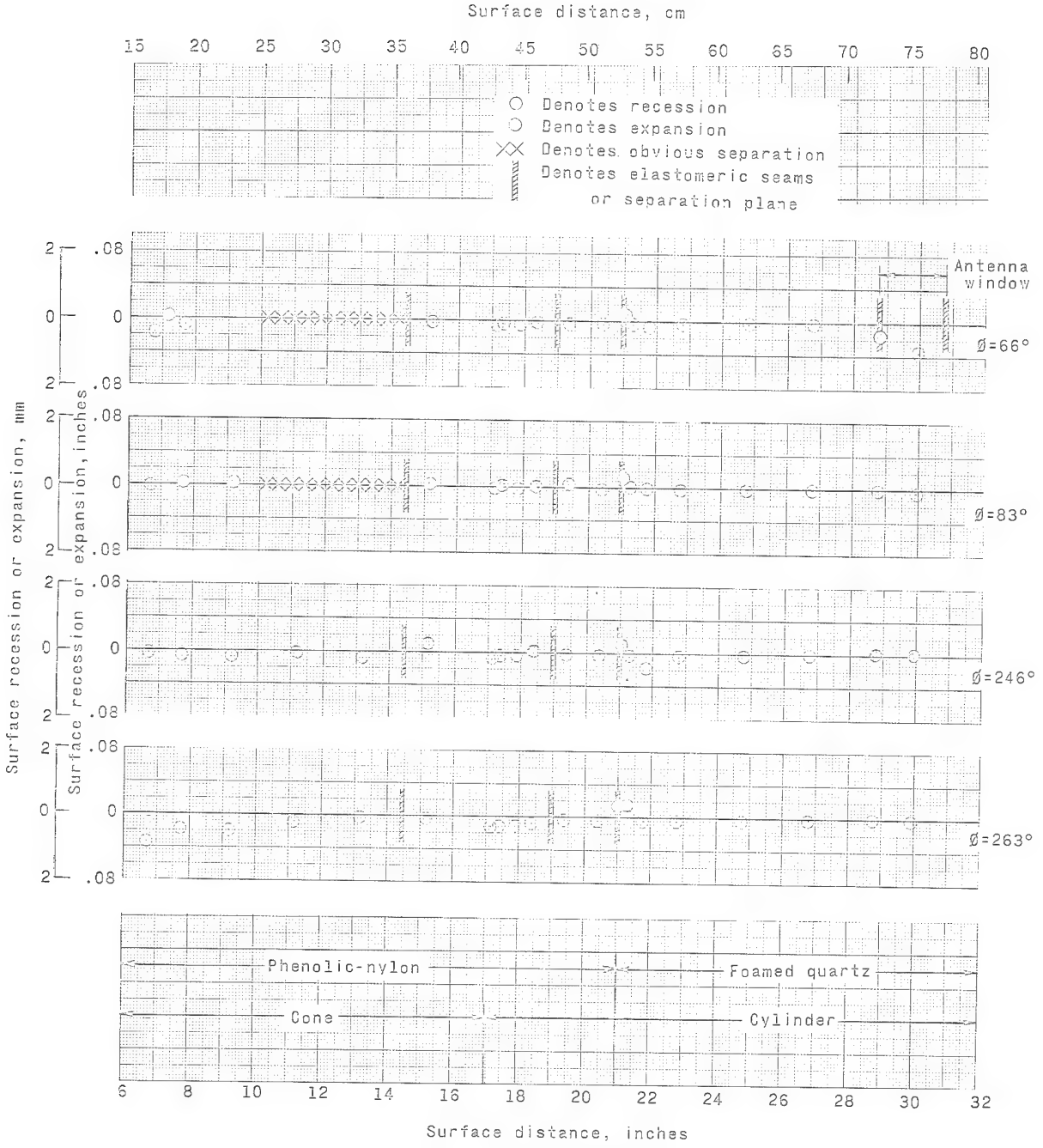

(c) Cone and cylinder (Ø = 66°, 83°, 246°, and 263°).

Figure 19.- Continued.

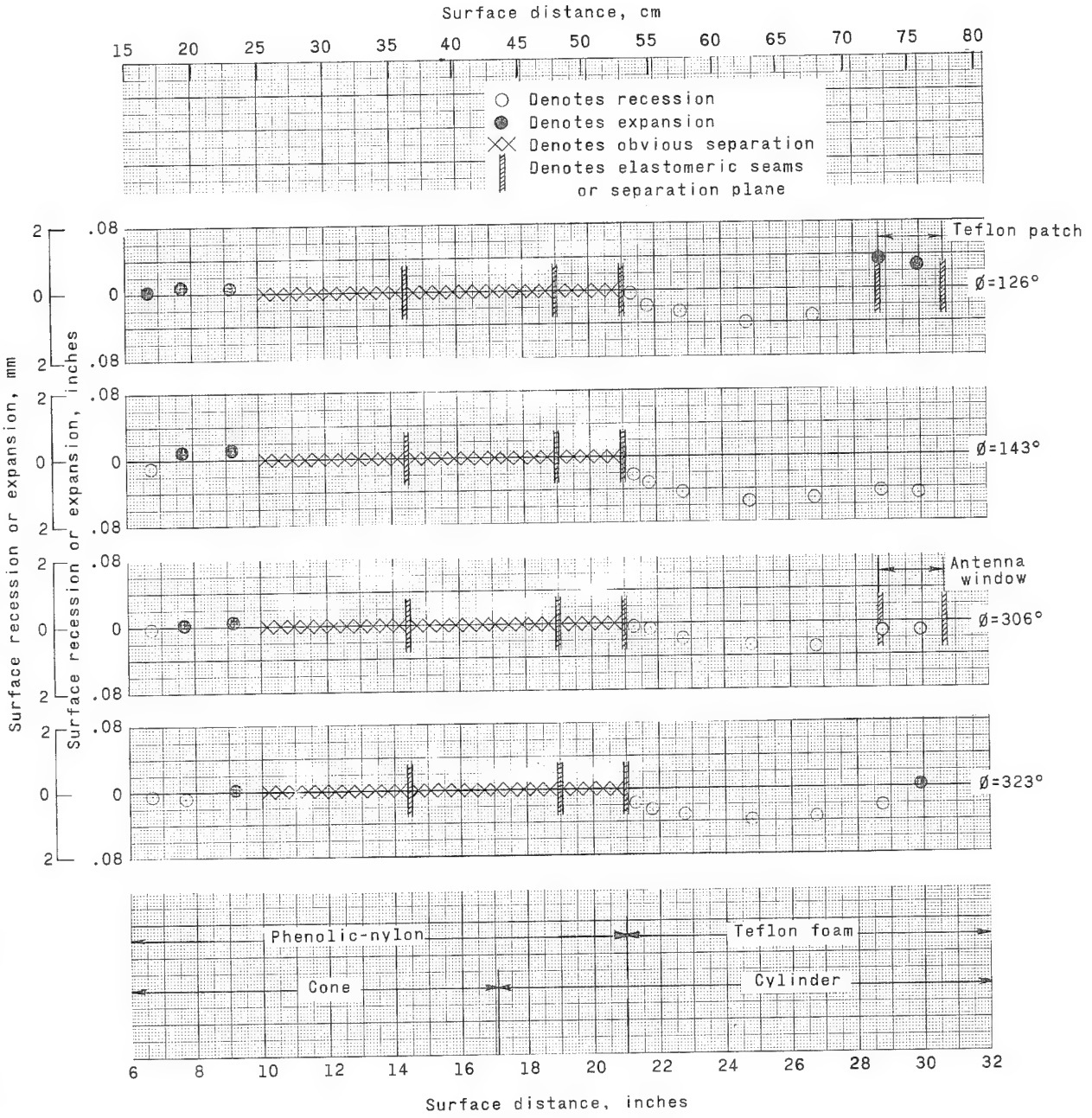

(d) Cone and cylinder (Φ = 126°, 143°, 306°, and 323°).

Figure 19.- Concluded.

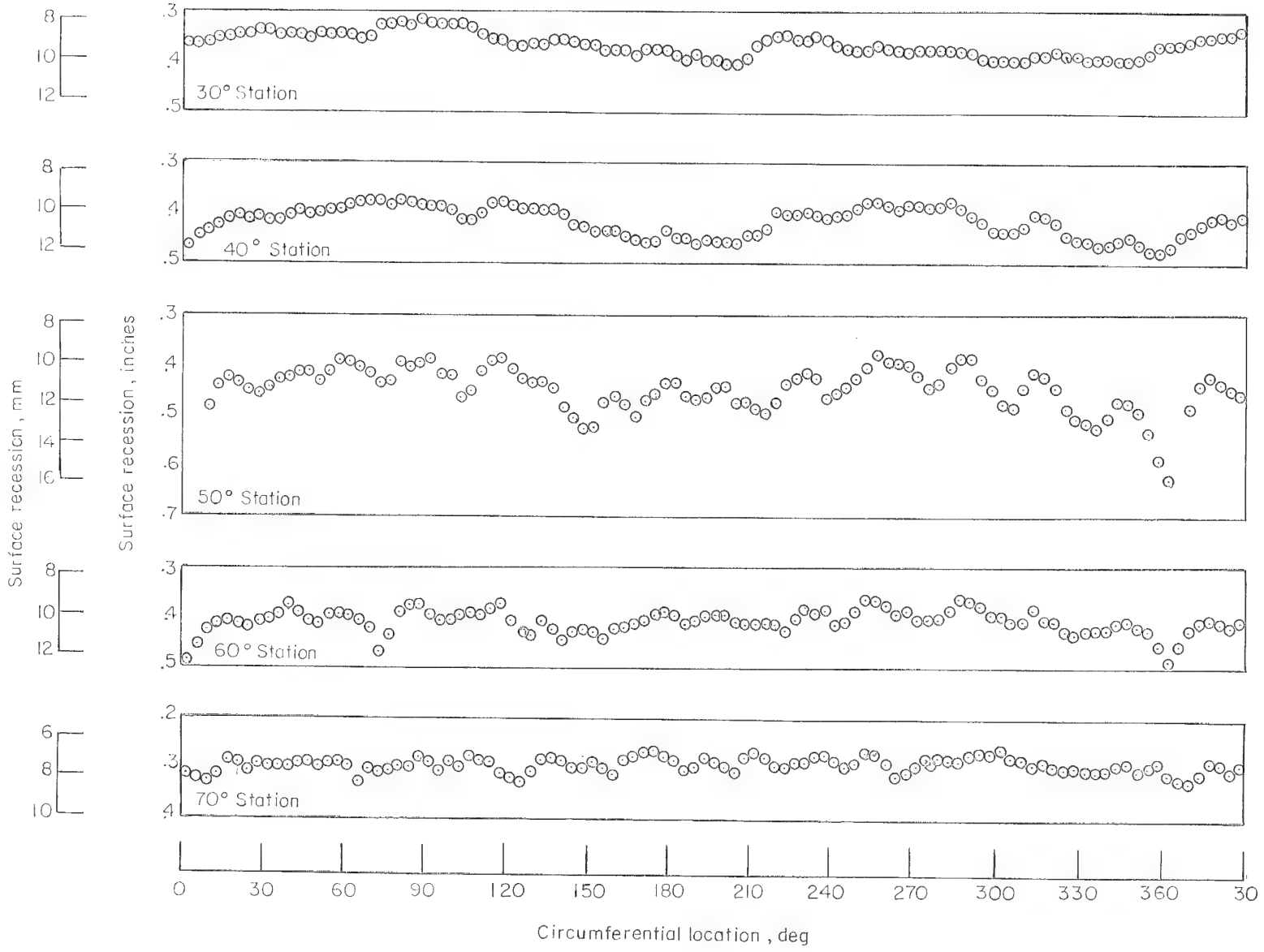

Figure 20.- Surface-recession measurements around the 30^0, 40^0, 50^0, 60^0, and 70^0 stations on the hemisphere.

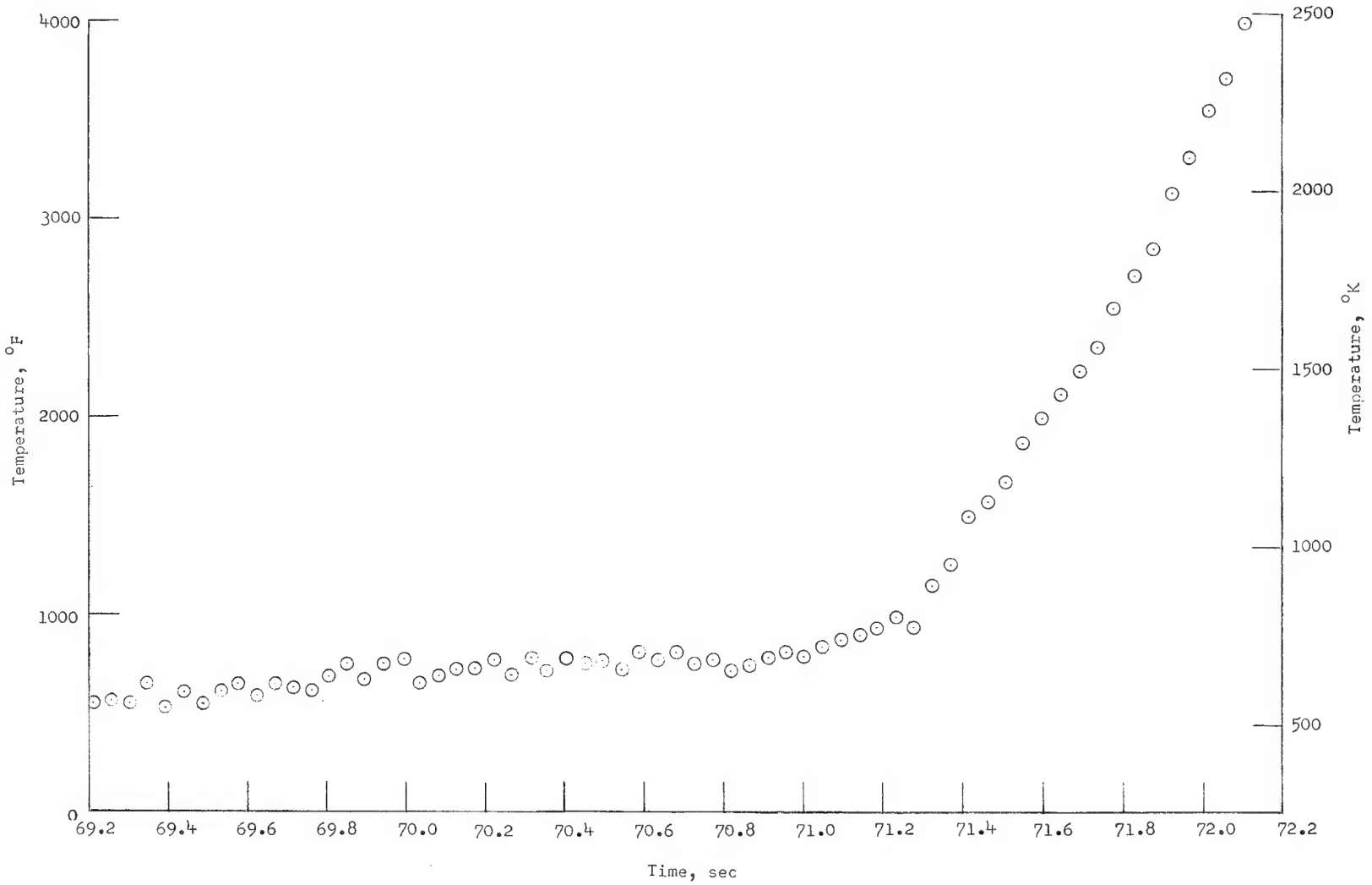

Figure 21.- Surface temperature-time history at 45^0 station, with every data point between 69.2 and 72.2 seconds plotted.

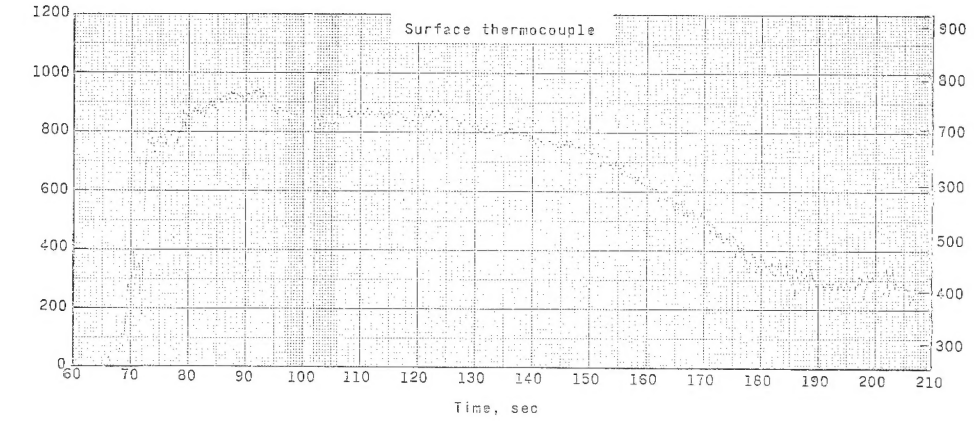

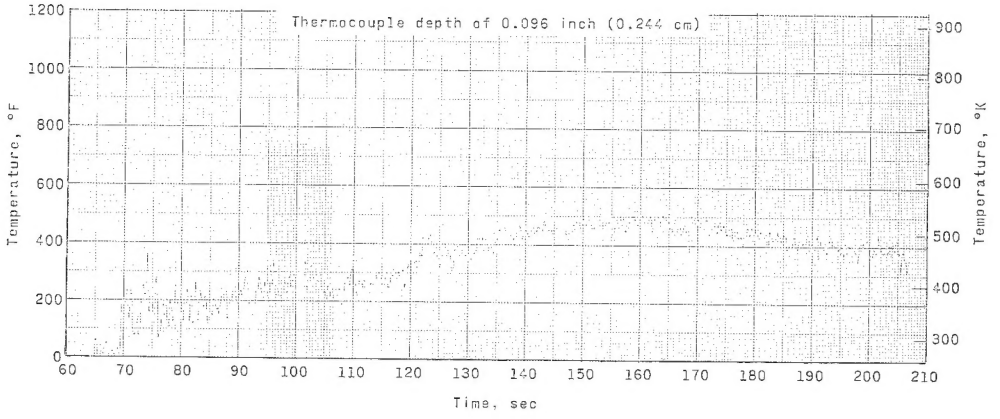

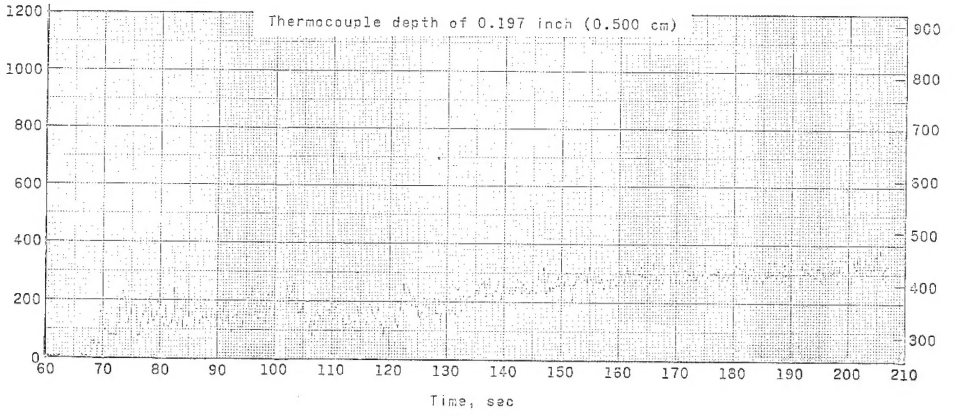

(a) Cone station 1.

Figure 22.- Temperature-time histories obtained from surface and in-depth thermocouples.

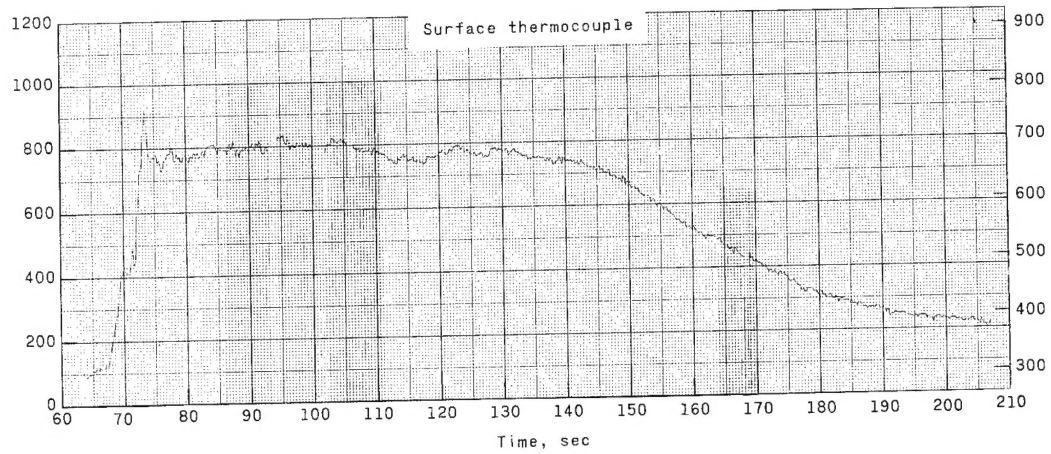

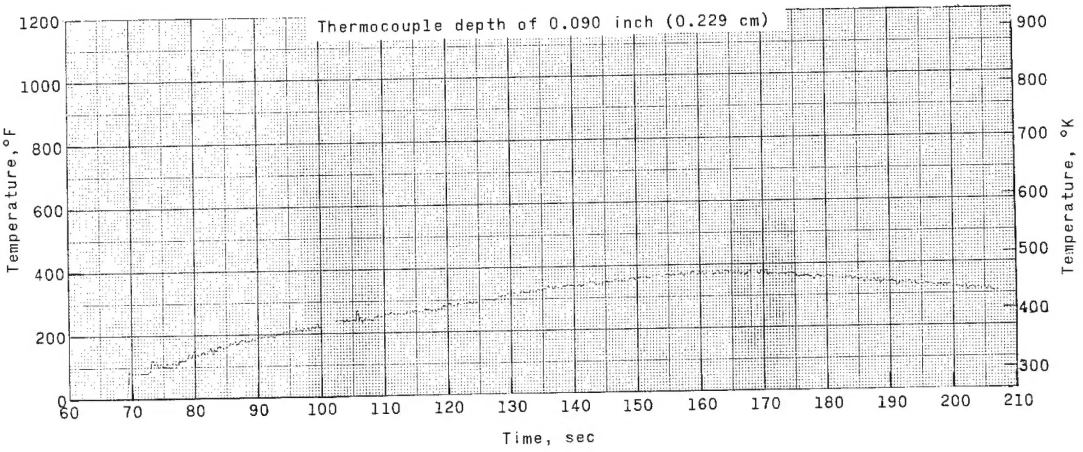

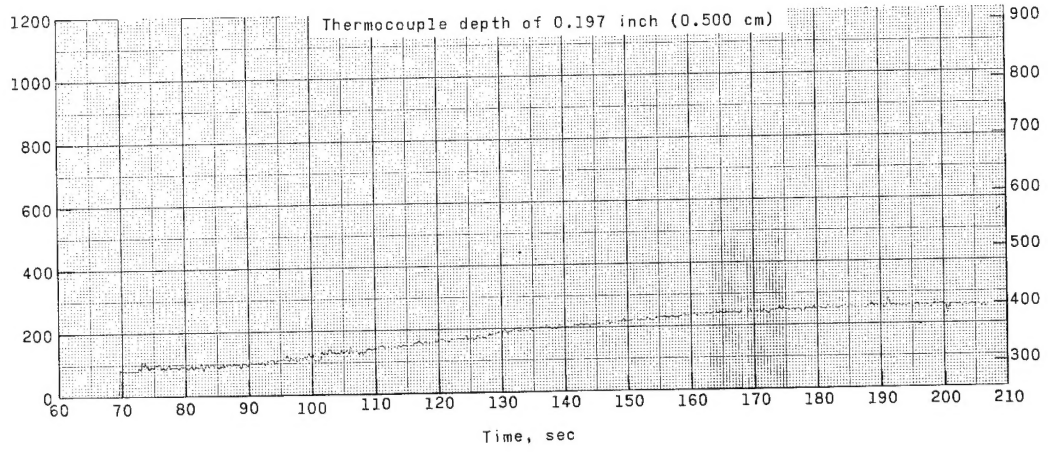

(b) Cone station 2.

Figure 22.- Continued.

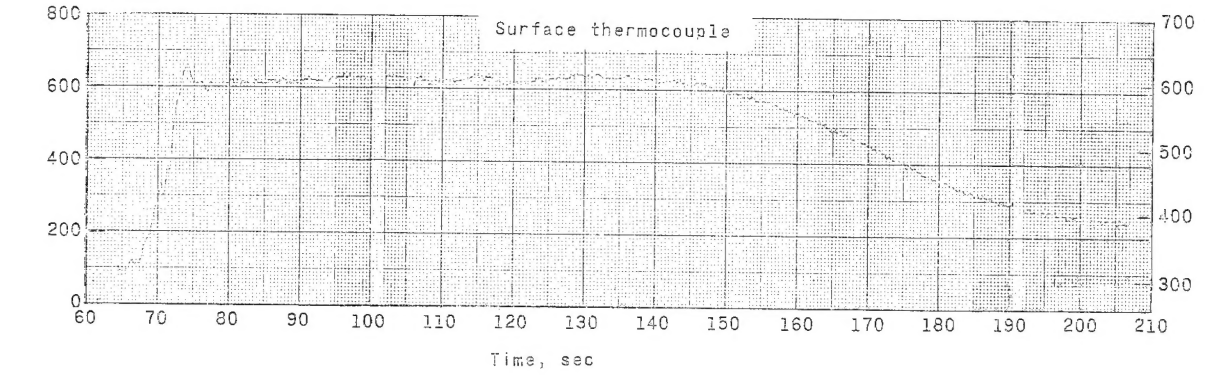

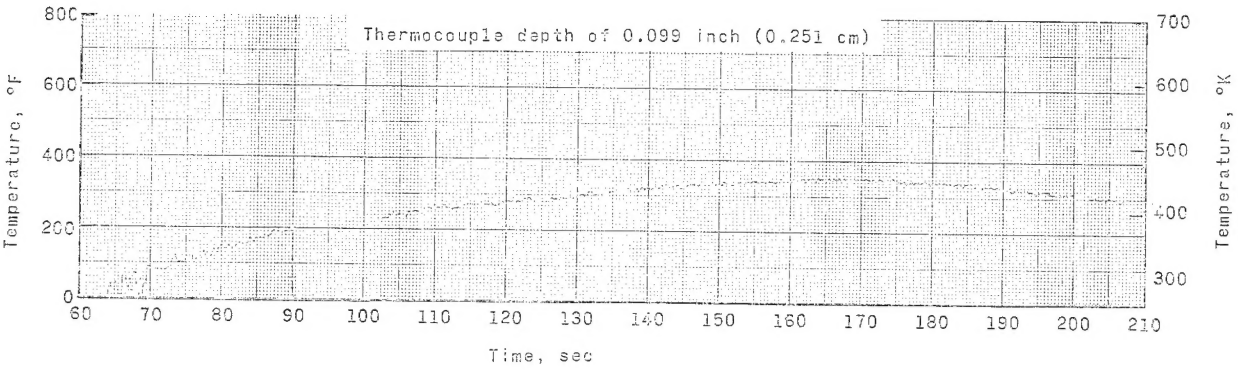

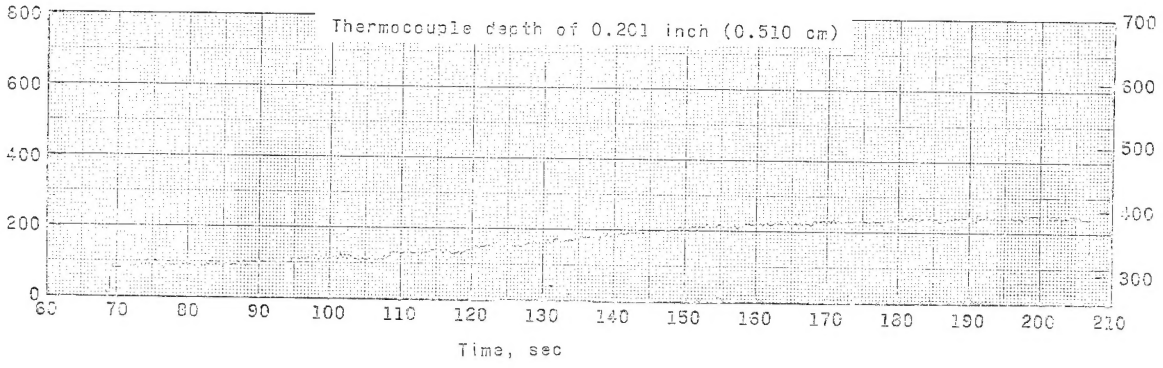

(c) Cylinder station 1.

Figure 22.- Concluded.

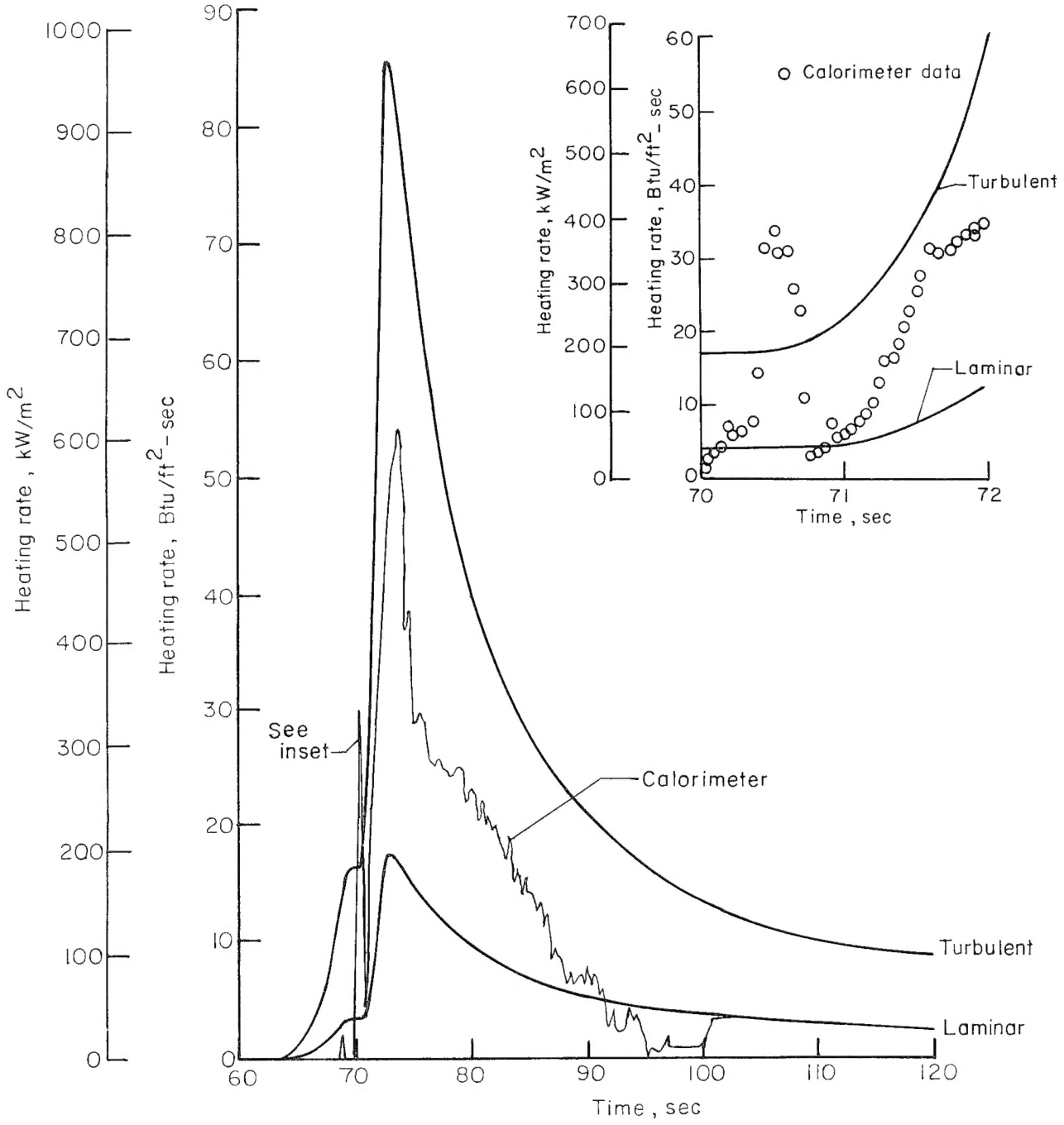

Figure 23.- Computed laminar and turbulent heating rates superimposed on heating rates for calorimeter C-1 at cylinder station 1.